The Canadian Mineralogist
Vol. 46, pp. 1593-1622 (2008)
DOI: 10.3749/canmin.46.6.1593

POWDER NEUTRON-DIFFRACTION STUDIES OF CLINOPYROXENES. I. THE CRYSTAL STRUCTURE AND THERMOELASTIC PROPERTIES OF JADEITE BETWEEN 1.5 AND 270 K

KEVIN S. KNIGHT

ISIS Facility, Rutherford Appleton Laboratory, Chilton, Didcot, Oxon., OX11 0QX, and Department of Mineralogy, The Natural History Museum, Cromwell Road, London, SW7 5BD, U.K.

G. DAVID PRICE

Department of Earth Sciences, University College London, Gower Street, London, WC1E 6BT, U.K.

ABSTRACT

The crystal structure of pure jadeite has been determined by Rietveld refinement of powder neutron-diffraction data at 28 temperatures between 2.5 and 268 K, allowing a structural basis for the thermal expansion that is proposed. Characteristic temperatures for the thermal expansion and the atomic displacement parameters have been derived from the experimental data using either Debye or Einstein formalisms and are found to be in broad agreement with calorimetric measurements and mode assignments from vibrational spectroscopy. The temperature dependence of the thermodynamic Grüneisen parameter shows it to be small, less than unity, in agreement with that in other pyroxene phases.

Keywords: jadeite, $NaAlSi_2O_6$, crystal structure, neutron diffraction, thermoelastic properties.

SOMMAIRE

Nous avons déterminé la structure cristalline de la jadéite pure par affinement de Rietveld de données obtenues par diffraction de neutrons à 28 températures allant de 2.5 à 268 K, ce qui nous a permis d'établir une base structurale de l'expansion thermique proposée. Les températures caractéristiques pour l'expansion thermique et les paramètres décrivant les déplacements des atomes ont été dérivés à partir des données expérimentales au moyen des formalismes de Debye ou de Einstein; ils concordent en général avec les mesures calorimétriques et les modes assignés selon la spectroscopie vibrationnelle. D'après la dépendance du paramètre thermodynamique de Grüneisen sur la température, ce paramètre aurait une petite valeur, moins de un, tout comme pour les autres membres de la famille des pyroxènes.

(Traduit par la Rédaction)

Mots-clés: jadéite, $NaAlSi_2O_6$, structure cristalline, diffraction de neutrons, propriétés thermoélastiques.

INTRODUCTION

In 1925, Wyckoff *et al.* demonstrated that jadeite is isostructural with diopside using powder X-ray diffraction, and some forty years later, Prewitt & Burnham (1966) determined the crystal structure at room temperature from single-crystal data. A study of the temperature dependence of the crystal structure of jadeite at four temperatures (297, 673, 873 and 1073 K) was subsequently made by Cameron *et al.* (1973) as part of the first definitive crystallographic study of the clinopyroxene family at high temperatures. However, since this time, crystallographic work on pyroxenes containing a significant mole fraction of jadeite has been more focused on an understanding of the omphacite (jadeite–diopside) solid solution than on the end-member component itself. The reduction in space-group symmetry from *C*2/*c* to *P*2/*n* in the omphacitic pyroxenes results in two independent tetrahedral sites within a single chain and in two independent octahedral sites. This increase in the number of degrees of freedom for the *P*2/*n* structure over the *C*2/*c* structure makes a simple parameterization of structural changes in temperature or pressure more difficult to disentangle

§ *E-mail address*: kevin.knight@stfc.ac.uk

and determine with precision. For simplicity, we have therefore made our initial investigation of the structural parameterization of clinopyroxenes at low temperature by studying the end-member phase, jadeite.

Whereas there is little direct relevance of such low-temperature pyroxene crystallography to terrestrial geology, some of the earliest results from the Infrared Space Observatory (ISO) have shown the presence of crystalline silicates outside the solar system and at temperatures below 150 K (Bowey *et al.* 2001, Molster *et al.* 2002a, b, c). Before the launch of ISO, it had been generally assumed that only amorphous silicates were formed in the dusty winds of O-rich evolved stars, but the mid- and far-infrared spectrometers on ISO have shown the presence of crystalline silicates, not only in the spectra of young stellar objects, but also in comets and in the oxygen-rich dust in outflows and discs of evolved stars. Comparison with laboratory spectra has suggested that forsterite and orthoenstatite are the dominant phases, with some evidence being found for diopside and clinoenstatite (Molster *et al.* 2002b). Unfortunately, phase identification is rendered difficult because the reference spectra were collected at room temperature, whereas the emission bands from the dust are associated with temperatures probably of the order of 150 K (Bowey *et al.* 2001), but possibly even as low as 50 K (Sylvester *et al.* 1999). With current techniques of modeling, one is not yet capable of determining the temperature dependence of these emission bands for pyroxenes, but clearly, knowledge of the crystal structures will be a necessary prerequisite for such calculations. There is therefore a need for low-temperature structural characterization of the potential astromineralogical silicate phases. In this paper, the first in a series of structural studies of natural and synthetic clinopyroxenes determined by powder neutron diffraction, the crystal structure, thermal expansion, Debye and Einstein characteristic temperatures and Grüneisen parameters for jadeite are reported from 1.5 to 270 K.

Background Information

The advantages of carrying out crystallographic studies on minerals at ultra-low temperatures far outweigh the experimental difficulties in data collection, as it allows a number of thermodynamic parameters that are generally difficult to measure directly to become easily accessible. Provided data exist for both the heat capacity and the bulk modulus, the measurement of the unit-cell volume as a function of temperature allows the temperature variation of the thermodynamic Grüneisen parameter to be determined and good estimates to be made for both the Einstein and Debye temperatures (Wood *et al.* 2002, Vočadlo *et al.* 2002a, b, Fortes *et al.* 2005). At low temperatures, the effects of the librational modes of the constituent polyhedra are minimized, and hence the determination of the temperature dependence of bond lengths is not compromised by the use of traditional techniques of data analysis that solely rely on Bragg scattering to determine atomic coordinates. This is in marked contrast to high-temperature crystallographic studies on materials containing librating polyhedra that exhibit large displacements of atoms. In the high-temperature case, the determination of the instantaneous, rather than the time-averaged, shortened bond-lengths requires total scattering techniques that utilize both the Bragg scattering and the diffuse scattering in the data analysis (Tucker *et al.* 2000). At low temperatures, the precise measurement of atomic displacement parameters allows the determinations of the zero-point displacements and the vibrational Debye temperatures to be made from fitting the measured temperature dependences to simple lattice-dynamical models (Wood *et al.* 2002).

Collections of single-crystal X-ray-diffraction data made at temperatures significantly lower than 77 K, liquid nitrogen temperature, are difficult to perform and still remain a somewhat specialized activity. By contrast, neutron single-crystal and powder diffraction are routinely carried out from temperatures of 1.2 K, with temperatures as low as 30 mK readily achievable in ^{3}He/^{4}He dilution inserts. The choice of which neutron technique to use is, of course, sample-dependent, and with a lack of suitably large crystals of jadeite, plus the requirement for rapid collections of data in this study, powder diffraction was the technique of choice.

With the exceptions of the single-crystal neutron-diffraction study of diopside made at 10 K (Prencipe *et al.* 2000), spodumene at 54 K (Tribaudino *et al.* 2003) and the X-ray diffraction investigation of $NaGaSi_2O_6$ between 110 and 295 K (Nestola *et al.* 2007), almost all low-temperature structural studies of pyroxenes have been carried out using powder neutron diffraction on natural or synthetic systems that exhibit antiferromagnetic ordering (Herpin *et al.* 1971, Shamir & Shaked 1975, Wiedenmann & Regnard 1986, Wiedenmann *et al.* 1986, Ghose *et al.* 1988, Ballet *et al.* 1989, Lottermoser *et al.* 1998, Knight *et al.* 2000, Lumsden *et al.* 2000, Redhammer *et al.* 2001, Knight 2001a, b). In general, the particular aim of these measurements has been the elucidation of the magnetic structure of the pyroxene rather than an analysis of the nuclear structure at low temperatures. The detailed low-temperature investigation of the structure, magnetism and the $P2_1/c$ to $C2/c$ phase transition in the synthetic clinopyroxene $LiFeSi_2O_6$ by Redhammer *et al.* (2001) is probably the most notable exception.

Experimental Methods and Data Reduction

Sample details

A monominrealic sample of jadeite was cut from a small white boulder from the Hweka and Mamon mining district of Burma, bearing Natural History Museum catalogue number BM 1913,451. Part of the

cut slice was broken up in a percussion mill before being ground under acetone with an agate pestle and mortar and sieved to <75 μm to produce a sample suitable for powder neutron diffraction. Electron-microprobe analysis at 24 points on a small representative fragment gave an average composition of essentially pure jadeite, $NaAlSi_2O_6$, with only traces of Mg, Ca and Fe being determined at some of the sampled points. In addition, Ti, Cr, Mn and K were sought, but were not detected. The sample composition was therefore assumed to be ideal in the subsequent data-reduction and analysis, including the corrections for self-shielding and absorption applied to the powder neutron-diffraction data used in profile refinement.

Neutron diffraction

Powder neutron-diffraction data were collected using two time-of-flight diffractometers, HRPD and POLARIS, at the ISIS neutron spallation source of the Rutherford Appleton Laboratory, U.K. As the low-temperature thermal expansion behavior of a number of natural pyroxenes has been found to exhibit subtle features, *e.g.*, magnetostriction below the Néel temperature in aegirine and hedenbergite (Knight *et al.* 2000, Knight 2001b, data at the highest resolution ($\Delta d/d = 4 \times 10^{-4}$) were collected on HRPD to determine the temperature dependence of the unit-cell parameters. The results from these data have been used to determine both the temperature dependences of the thermal expansion tensor and the thermodynamic Grüneisen parameter, but also to calibrate the lower-resolution measurements made with POLARIS. In addition, they have been used to estimate both the Einstein and Debye temperatures for jadeite from the variation of the unit-cell volume with temperature. Data of structure-refinable quality were collected on the medium-resolution ($\Delta d/d = 5 \times 10^{-3}$) high-flux diffractometer POLARIS.

For the HRPD measurements, 4 cm^3 of jadeite powder was lightly packed in an aluminum sample can of slab geometry with thin, neutron-transparent, vanadium front and back windows. Heat was supplied to the sample through a 100 W cartridge heater inserted in the side wall of the sample can, and the temperature was monitored through a Rh/Fe sensor located in the opposite wall. To ensure a good thermal contact with the sample can, the heater and sensor were smeared with Jet-Lube SS–30, a copper-containing anti-seize compound. A gadolinium neutron-absorbing mask was attached to the side of the can facing the back-scattering detectors and the incident beam to prevent contaminant Bragg peaks arising from both the body of the sample can, including sensor and heater, and the stainless steel frames supporting the vanadium windows. The entire assembly was attached to a center stick and located in an AS Scientific "Orange" helium cryostat 50 mm in diameter. The sample was slowly cooled to 4.2 K under 30 mbar of helium exchange gas before being pumped down to a stable base temperature of 1.5 K. Data were collected at 1.5 K, 5 K and in 5 K steps to 50 K, thereafter in 10 K steps to 270 K. Data in the time-of-flight window 40 – 140 ms, corresponding to a range in d of 0.8 to 2.8 Å in the back-scattering detectors, were collected for a total of 8 μAh with a 5-minute thermal equilibration step between measurements. On average, each measurement took approximately 30 minutes to complete. The data from the back-scattering detectors were focused to a mean flight-path of 95.8924 m and Bragg angle of 168.329° 2ϑ, background-subtracted, normalized to the distribution of incident flux using an upstream monitor and corrected for detector efficiency using a vanadium standard. Data in the time-of-flight range 42 – 130 ms, binned logarithmically as $\Delta t/t = 3 \times 10^{-4}$, were used in cell and intensity least-squares refinement (Pawley 1981) to determine the temperature variation of the unit-cell parameters.

For the POLARIS measurements, 8.5 g of jadeite powder was lightly packed into a cylindrical vanadium sample can 11 mm in internal diameter, and cooled to 4.2 K using an identical cryostat to that used in the HRPD measurements. The cryostat was then pumped to achieve a stable base temperature of 2.5 K. Data were collected at 2.5 K for 400 μAh, then 10 K for 200 μAh, and thereafter in 10 K steps to 280 K for 200 μAh. Between each data-collection point, a ten-minute thermal equilibration step was performed, and the total time to collect an individual temperature point was of the order of 75 minutes. The quoted temperatures represent the controlling set point for the cryostat; the average temperature of the sample during data collection was determined by integrating the temperature log file for the Rh/Fe sensor in the cryostat center-stick located close to the top of the sample can. Data from two detector banks with mean Bragg angles of 2ϑ = 145° and 90° were focused, cryostat-background-subtracted and normalized to the distribution of the incident flux using a vanadium standard. These two datasets were then corrected for self-shielding and wavelength-dependent absorption for a sample of pure jadeite composition, a measured number density of 5.44×10^{21} cm^{-3}, and calculated cross-sections of 34.51 b for scattering and 1.10 b, at a wavelength of 1.798 Å, for absorption (Sears 1992). Data, binned logarithmically as $\Delta t/t = 5 \times 10^{-4}$ in the time-of-flight range 2 – 18.0 ms for 2ϑ = 90°, and 2 – 19.6 ms for 2ϑ = 145°, were used in Rietveld profile analysis.

Data Analysis of Lattice Parameters and Unit-Cell Volume

Unit-cell parameters

On cooling to 1.5 K, the data in all three diffraction detector banks of HRPD (168.329°, 90.0°, 30.0° 2ϑ) were carefully scrutinized for evidence of loss of either the lattice centering or the glide plane. No additional

reflections were observed in the data, and hence the space group of jadeite remains unchanged from that at ambient temperature, namely *C*2/*c*. The temperature dependence of the unit-cell parameters was determined by cell and intensity least-squares refinement (Pawley 1981) of the HRPD data, as implemented in the Rietveld refinement program TF12LS (David *et al.* 1992), which is based on the Cambridge Crystallographic Subroutine Library, CCSL (Brown & Matthewman 1993). This program allows a structural-model-free fit to neutron time-of-flight data in which the integrated intensity of each reflection, subject to the constraints described in detail by Pawley (1981), the lattice constants, the peak-shape function and instrumental parameters form the variables to be refined. In this method, the whole diffraction pattern, to the maximum resolution in d^* that has been measured, contributes to the final estimated standard deviations of the lattice parameters. The method is therefore free of the systematic errors and bias that can arise from the selection of a small number of reflections and using a conventional least-squares unit-cell refinement. A trial unit-cell for jadeite at 1.5 K was derived from the ambient-temperature lattice parameters of Cameron *et al.* (1973), and the 1.5 K data were fitted using a peak shape described by the Robinson–Taylor–Carpenter function, a convolution of a Voigt function with a double exponential decay and switch function. The background was modeled by a 10-term Chebychev polynomial of the first kind. During the refinement, it was only found necessary to refine the quadratic wavelength dependence of the Gaussian variance and the linear wavelength dependence of the Lorentzian component of the Voigt function. Analysis of the 280 K data was performed next and showed that these two line-width terms were independent of temperature within estimated standard deviations. They were therefore fixed at the 1.5 K values for all subsequent refinements in which the refined values of the unit cell at one temperature were used as the starting values for the next temperature. The refinement for the 1.5 K data converged with $\chi^2 = 1.1$ for 301 variables with a similar goodness of fit being found for all the datasets analyzed. An example of the quality and fit of the data is shown in Figure 1 for the data collected at 1.5 K, for which the refined lattice parameters are a = 9.41582(9), b = 8.55515(4), c = 5.22071(21) Å and β = 107.5634(7)°. The temperature dependence of the unit-cell parameters between 1.5 and 270 K is shown in Figure 2 and listed in Table 1.

All three axial lengths show the expected dependence on temperature obeying Grüneisen's law both at low temperature, where the thermal expansion coefficient tends to zero magnitude, and at higher temperature, where the thermal expansion coefficient is beginning to tend to a constant value. By contrast with the axial variations, the beta angle showed an unexpected sigmoidal variation with temperature, exhibiting saturation behavior at both low temperature and at temperatures greater than 200 K. This observation, close to room temperature, is in good agreement with the high-temperature results of Cameron *et al.* (1973), who found no significant variation in the beta angle of jadeite with temperature from 297 to 1073 K.

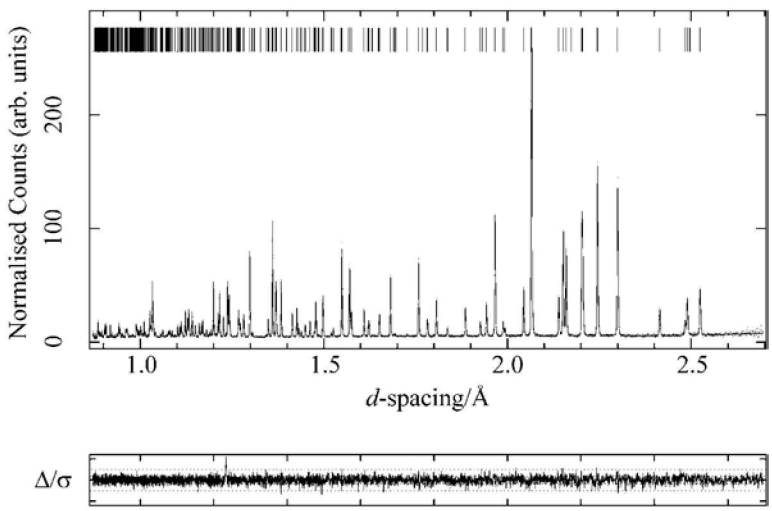

FIG. 1. Cell and intensity least-squares fit to powder neutron-diffraction data for jadeite collected at 1.5 K using HRPD. The observed data are points, and the full line shows the calculated pattern. The lower plot shows the difference between the observed data and the calculated pattern (Δ) divided by the estimated standard deviation of the observed data (σ). Values of $\pm 3\Delta/\sigma$ are shown as dotted horizontal lines on the difference plot.

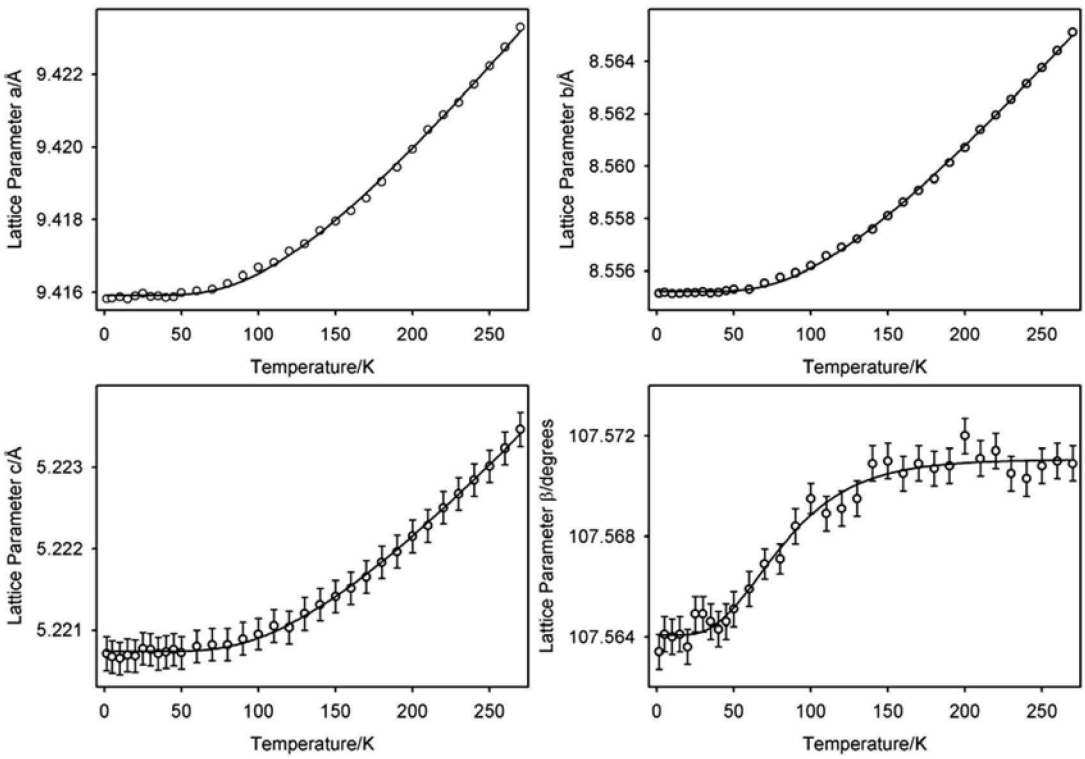

FIG. 2. The temperature dependence of the lattice parameters of jadeite between 1.5 and 270 K. For the three axial lengths, the full line shows the least-squares fit to these data according to an Einstein function. For the interaxial angle β, the full line shows a fit to a four-parameter Chapman sigmoidal function. For the unit-cell axes *a* and *b*, the estimated standard deviation of the unit-cell edges is smaller than the symbol used in the plot.

The unit-cell edges show a similar dependence on temperature to that of the unit-cell volume. For simplicity, they have been fitted using weighted least-squares to an Einstein expression of the form (Wallace 1972):

$$l(T) = l_0 + \frac{A_i}{e^{B_i/T} - 1}$$

where l_0 is the magnitude of the lattice parameter at 0 K, and A_i and B_i are refinable constants. The unusual behavior of the beta angle can be fitted to a similar expression to that given above, but in this case, it is necessary to introduce an additional temperature-dependent term with a negative A_i value. For beta to exhibit saturation at high temperatures, it is a necessary requirement for $\frac{A_1}{B_1} = -\frac{A_2}{B_2}$, which is clearly too much greater a constraint to be physically realistic, and hence for simplicity, the beta angle was fitted using weighted least-squares to an empirical four-parameter Chapman sigmoidal function of the form:

$$\beta(T) = \beta_0 + A\left(1 - e^{-BT}\right)^C$$

where β_0 is the magnitude of the beta angle at 0 K, and A, B and C are refinable constants.

One can see from the figure that both parameterizations give excellent descriptions of the temperature variation of the unit-cell parameters. The values of the refined parameters determined from the fitting procedure are listed in Table 2. One particular advantage of such simple parameterizations is that the magnitude of the thermal expansion coefficient of the individual lattice constants may be easily calculated for any temperature from above the saturation region up to the maximum temperature measured. In agreement with the earlier observations of Cameron *et al.* (1973), the relationship of $db/dT > da/dT > dc/dT$ holds for temperatures greater than ~40 – 50 K up to 270 K. If the expression for $\beta(T)$ is considered, one can see by inspection for $B > 0$,

TABLE 1. UNIT-CELL PARAMETERS OF JADEITE BETWEEN 1.5 AND 270 K

Temp.	*a*, Å	*b*, Å	*c*, Å	β, °
1.5	9.41582(9)	8.55515(4)	5.22071(21)	107.5634(7)
5.0	9.41583(9)	8.55518(4)	5.22067(20)	107.5641(7)
10.0	9.41587(9)	8.55513(4)	5.22065(20)	107.5640(7)
15.0	9.41581(9)	8.55514(4)	5.22069(20)	107.5641(7)
20.0	9.41590(9)	8.55517(4)	5.22068(20)	107.5636(7)
25.0	9.41597(9)	8.55517(4)	5.22077(20)	107.5649(7)
30.0	9.41588(9)	8.55521(4)	5.22076(20)	107.5649(7)
35.0	9.41590(9)	8.55516(4)	5.22071(20)	107.5646(7)
40.0	9.41585(9)	8.55518(4)	5.22073(20)	107.5643(7)
45.0	9.41587(9)	8.55525(4)	5.22076(20)	107.5646(7)
50.0	9.41598(9)	8.55530(4)	5.22072(20)	107.5651(7)
60.0	9.41604(9)	8.55531(4)	5.22080(20)	107.5659(7)
70.0	9.41608(9)	8.55554(4)	5.22082(20)	107.5669(6)
80.0	9.41624(9)	8.55577(4)	5.22082(20)	107.5671(6)
90.0	9.41646(9)	8.55593(4)	5.22089(20)	107.5684(7)
100.0	9.41668(9)	8.55619(4)	5.22095(19)	107.5695(6)
110.0	9.41681(9)	8.55657(4)	5.22105(20)	107.5689(7)
120.0	9.41713(9)	8.55690(4)	5.22103(20)	107.5691(7)
130.0	9.41733(9)	8.55722(4)	5.22120(20)	107.5695(7)
140.0	9.41770(9)	8.55759(4)	5.22131(20)	107.5709(7)
150.0	9.41795(9)	8.55810(4)	5.22141(20)	107.5710(7)
160.0	9.41824(9)	8.55863(4)	5.22151(20)	107.5705(7)
170.0	9.41859(9)	8.55908(4)	5.22165(20)	107.5709(7)
180.0	9.41904(9)	8.55952(4)	5.22183(20)	107.5707(7)
190.0	9.41944(9)	8.56013(4)	5.22196(20)	107.5708(7)
200.0	9.41994(9)	8.56071(4)	5.22215(20)	107.5720(7)
210.0	9.42047(9)	8.56139(4)	5.22228(20)	107.5711(7)
220.0	9.42089(9)	8.56195(4)	5.22250(20)	107.5714(7)
230.0	9.42123(9)	8.56256(4)	5.22267(20)	107.5705(7)
240.0	9.42172(9)	8.56314(4)	5.22284(20)	107.5703(7)
250.0	9.42229(9)	8.56376(4)	5.22301(20)	107.5708(7)
260.0	9.42275(9)	8.56441(4)	5.22323(20)	107.5710(7)
270.0	9.42330(9)	8.56511(4)	5.22346(21)	107.5709(7)

TABLE 2. COEFFICIENTS DERIVED FROM LEAST-SQUARES FITS TO THE TEMPERATURE VARIATION OF THE UNIT-CELL PARAMETERS

Cell parameter	l_0, Å	A, Å	B, K	
a	9.41591(3)	0.0194(9)	351(8)	
b	8.55521(1)	0.0235(7)	331(5)	
c	5.22073(5)	0.0091(5)	401(12)	
	β_0, °	A, °	B, K^{-1}	C
β	107.5641(2)	0.0070(3)	0.0298(41)	7.3(2.4)

$d\beta/dT \rightarrow 0$ as the temperature decreases toward 0 K or increases to high temperatures. At high temperatures, $\beta = \beta_0 + A$, *i.e.*, it is constant, as found by Cameron *et al.* (1973). For the unit-cell edges at high temperatures, a linear Taylor's expansion of the exponential in the parameterization used in the lattice parameter fitting shows that $1/l_0\, dl/dT \rightarrow A/Bl_0$, thus giving an estimate of the high-temperature thermal-expansion coefficients on lattice parameters. Comparing these asymptotic values with the high-temperature measurements of lattice parameters of jadeite by Cameron *et al.* (1973) (which are given in parentheses), we find $1/a_0\, da/dT = 5.7(3) \times 10^{-6}\ K^{-1}$ ($8.3 \times 10^{-6}\ K^{-1}$), $1/b_0\, db/dT = 8.3(3) \times 10^{-6}\ K^{-1}$ ($1.00 \times 10^{-5}\ K^{-1}$), $1/c_0\, dc/dT = 4.3(3) \times 10^{-6}\ K^{-1}$ ($5.7 \times 10^{-6}\ K^{-1}$) and $d\beta/dT = 0\ K^{-1}$ ($0\ K^{-1}$). The agreements between these two sets of measurements are at best only fair, and the discrepancies probably arise from three sources. Firstly, only a limited range in temperature was measured in our study, and data measured up to the Debye temperature would probably improve the determination of the constants A and B. Secondly, the estimated standard deviations of the lattice parameters determined from the single-crystal study are relatively poor by comparison with those derived from the powder neutron-diffraction study, resulting in large uncertainties in the calculated thermal expansivity from the single-crystal measurements. Finally, and probably most importantly, there is the influence of anharmonicity, which will undoubtedly be present in the highest-temperature single-crystal datasets. Owing to this effect, the high-temperature thermal expansion coefficients would be expected to exhibit higher-order terms than only the linear term that has been assumed for comparative purposes.

Thermal expansion tensor

As one advantage of the parameterizations used for the cell-parameter characterization, the differentials of these functions are also simply evaluated, and hence allow the temperature dependence of the thermal expansion tensor to be computed readily (Knight 1996, Knight *et al.* 1999). Using the Institute of Radio Engineers convention for the cartesian tensor basis: $\mathbf{e_3} \parallel \mathbf{c}$, $\mathbf{e_2} \parallel \mathbf{b^*}$, $\mathbf{e_1} \parallel \mathbf{e_2} \times \mathbf{e_3}$, a monoclinic compound with *b* as the unique axis has thermal expansion tensor coefficients given by:

$$\alpha_{11}(T) = \frac{1}{a_0 \sin\beta_0}\left[\sin\beta\frac{da}{dT} + a\cos\beta\frac{d\beta}{dT}\right]$$

$$\alpha_{22}(T) = \frac{1}{b_0}\frac{db}{dT}$$

$$\alpha_{33}(T) = \frac{1}{c_0}\frac{dc}{dT}$$

$$\alpha_{12}(T) = 0$$

$$\alpha_{13}(T) = \frac{1}{a_0}\frac{da}{dT}\left[\frac{1}{\sin 2\beta_0} - \frac{\sin\beta}{2\cos\beta_0}\right] - \frac{a\cos\beta}{2a_0\cos\beta_0}\frac{d\beta}{dT} - \frac{\cot\beta_0}{2c_0}\frac{dc}{dT}$$

$$\alpha_{23}(T) = 0$$

Using the refined parameters from the least-squares fits to the temperature variation of the lattice constants, the temperature dependence of the thermal expansion tensor from 1 to 275 K was calculated using the expressions above. Figure 3 shows the calculated variation with temperature of the four-expansion tensor coefficients, which all exhibit the expected Grüneisen behavior of being zero at the lowest temperatures and progressively trending to a saturated value at higher temperatures. The magnitudes of the principal axes of the tensor (α_{ii}') were calculated for temperatures above 80 K by solving the eigenvalue problem analytically, and are shown in the lower part of Figure 3, with Ψ defined to be the angle between the eigenvector of α_{33}' from $\mathbf{e_3}$ toward $\mathbf{e_1}$. The calculations were carried out for temperatures greater than 80 K for two reasons; firstly, at this temperature, the lattice-parameter data recognizably move off the saturation base-line, and secondly, the parameterization behaves non-physically at much lower temperatures, leading to artefacts in the magnitudes of the tensor components. A similar observation of non-physical behavior in the components of

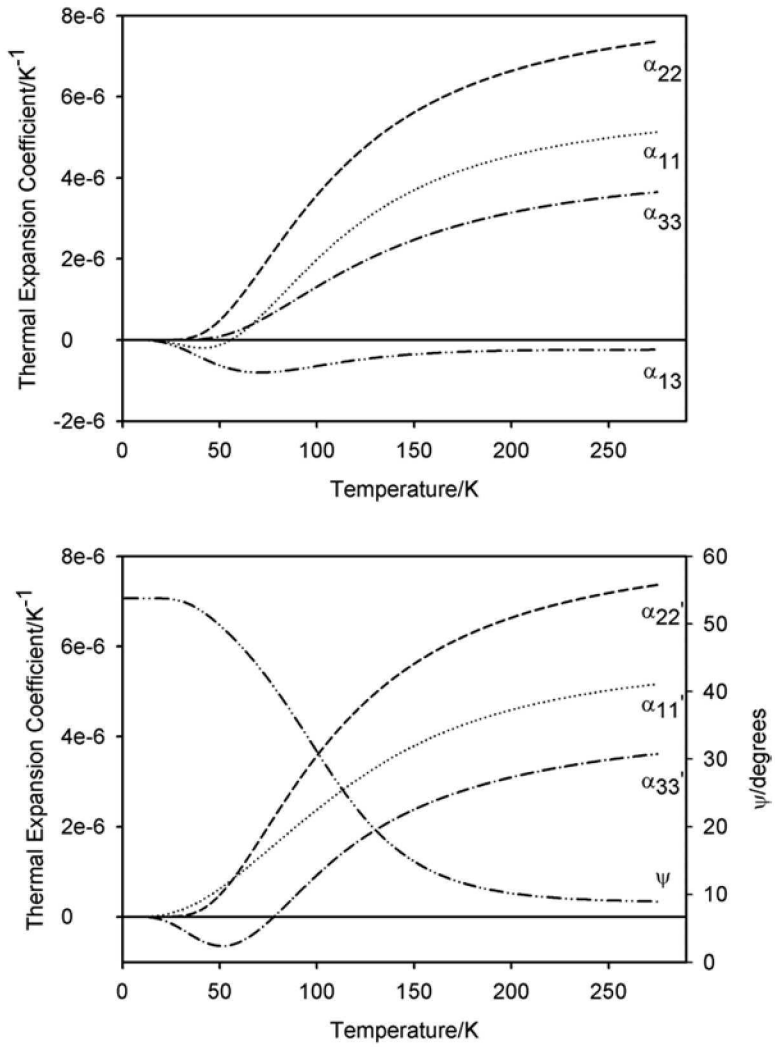

FIG. 3. Upper: The temperature dependence of the thermal expansion tensor for jadeite derived from the fitted temperature-variation of the lattice parameters. Lower: The temperature dependence of the principal axes of the thermal expansion tensor and the orientation angle Ψ (defined in the text).

the thermal expansion tensor at very low temperatures has been found in perdeuterated gypsum, which was attributed to the unusual oscillatory behavior of the β angle with temperature in this material (Knight *et al.* 1999). In general, the Einstein parameterization for the cell edges fails to give acceptable behavior for the thermal expansion coefficients at temperatures close to, or lower than, the saturation temperature because its derivative reduces far too rapidly with decreasing temperature than is observed experimentally. At the lowest useable temperature, the orientation of the minimum principal axis, α_{33}', is close to the direction determined for the minimum principal axis in diopside determined at high temperatures (Finger & Ohashi 1976). Using the bond nomenclature in clinopyroxene of Burnham *et al.* (1967), the orientation of α_{33}' is close to the projection of the *M*2 – O2*C*2/O2*D*2 bond onto the **a** – **c** plane, this bond length being the longest of the six shorter *M*2 – O bonds in jadeite. In contrast, in the case of diopside, this is the shortest of the six bonds. However, as the temperature increases from 80 K, α_{33}' moves away from $\mathbf{e_1}$ toward $\mathbf{e_3}$, eventually becoming essentially saturated at ~10° by 200 K. This saturated orientation is very close to the projection onto the **a** – **c** plane of the sum of the four bond vectors from *M*2 to O2*D*2, O1*A*1, O3*C*2 and O3*D*1. The change in Ψ mirrors the temperature dependence of the beta angle. It can be readily shown that at temperatures of the order of 100 K, dβ/dT is comparable in magnitude with both $1/c_0\ dc/dT$ and $1/a_0\ da/dT$. The magnitude of dβ/dT is present in the tensor expressions of both α_{11} and α_{13}, and therefore strongly influences the orientation of the principal axes in the **a** – **c** plane. The saturated orientation of the thermal expansion tensor and its relationship to both the crystal structure and the NaO_8 square antiprism are illustrated in Figure 4. One can see from the figure that the orientation of the principal axes of the tensor in jadeite lies closer to the intrinsic layering of the structural polyhedra than was found for diopside in Finger & Ohashi (1976).

Unit-cell volume, heat capacity and characteristic temperatures

Figure 5 shows the variation of the unit-cell volume with temperature and a fit to the data based on a Grüneisen approximation for the zero-pressure equation of state in which the effects of thermal expansion are considered to be equivalent to elastic strain (Wallace 1972). For low-temperature data with a limited range in temperature, as in this study, the volume scales with the internal energy, and to a first order:

$$V(T) = V_0 + \frac{\gamma U(T)}{K_0}$$

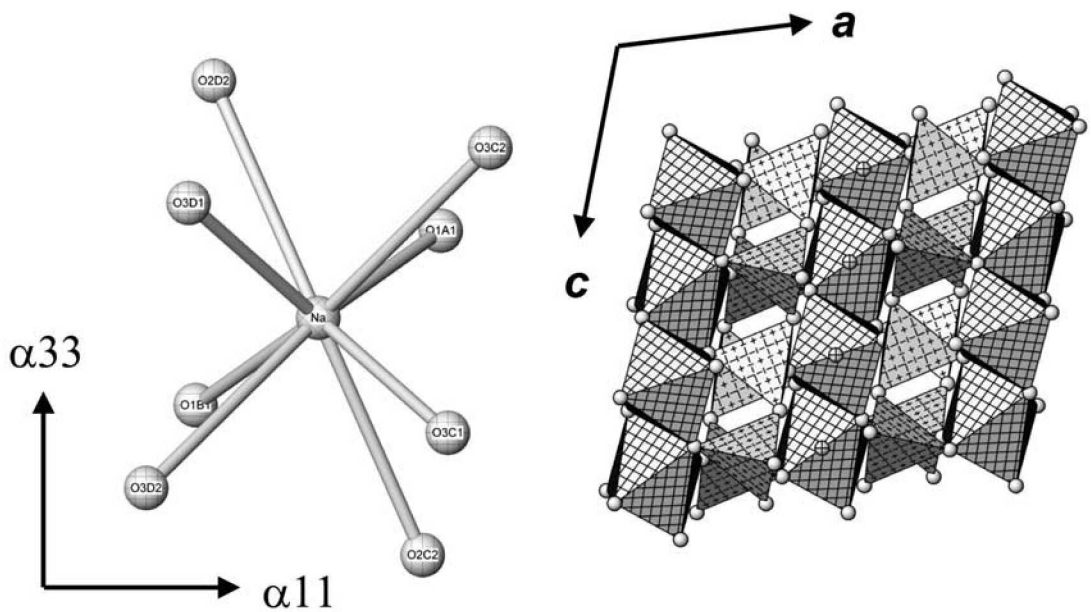

FIG. 4. Left: the saturated orientation of the principal axes of the thermal expansion tensor showing its relationship to the square-antiprismatic coordination of the NaO_8 polyhedron. Right: the relationship of the tensor to the structural layering in the crystal structure of jadeite.

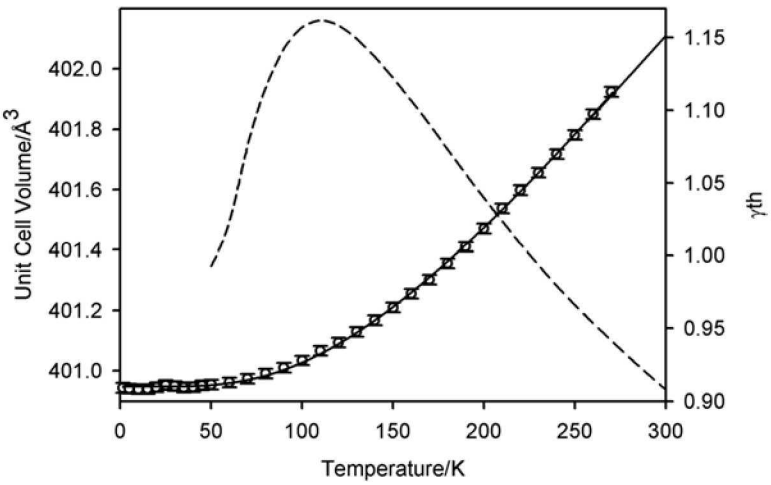

FIG. 5. The temperature variation of the unit-cell volume of jadeite, with the full line showing the results of fitting these data to a Debye model for the phonon density of states. The dashed line shows the calculated thermodynamic Grüneisen parameter for temperatures between 50 and 300 K. Over this whole interval of temperature, the Grüneisen parameter is seen to be low.

where γ' is a Grüneisen parameter, K_0 is the bulk modulus, and V_0 is the volume at 0 K. For simplicity, the internal energy U(T) may be calculated using either an Einstein approximation:

$$U(T) = \frac{3N\hbar\varpi_E}{e^{\hbar\varpi_E/k_BT}-1}$$

or the Debye approximation

$$U(T) = 9Nk_BT\left(\frac{T}{\vartheta_D}\right)^3\int_0^{\vartheta_D/T}\frac{x^3dx}{e^x-1}$$

where N is the number of atoms in the unit cell, k_B is Boltzmann's constant, ϑ_D is the Debye temperature, and the Einstein temperature, ϑ_E, is $\hbar\omega_E/k_B$. Both approximations give essentially indistinguishable fits to the data, with Figure 5 showing the results of the Debye fit. Weighed least-squares fitting gave $V_0 = 400.950(2)$ Å^3, $\vartheta_E = 369(6)$ K and $\gamma'/K_0 = 4.6(1) \times 10^{-12}$ Pa^{-1} for the Einstein approximation to the vibrational density of states, and $V_0 = 400.946(2)$ Å^3, $\vartheta_D = 539(7)$ K and $\gamma'/K_0 = 4.88(6) \times 10^{-12}$ Pa^{-1} for the Debye approximation. Using the measured bulk modulus for jadeite of 143(2) GPa (Kandelin & Weidner 1988) and the values of γ'/K_0 from the fitting procedure, approximate Grüneisen parameters can be calculated for jadeite, 0.66(2) in the Einstein approximation and 0.70(1) in the Debye approximation. More recent investigators of the bulk modulus of jadeite, determined by fitting the pressure dependence of the unit-cell volume to a third-order Birch–Murnaghan equation of state, have found slightly smaller values for the bulk modulus, 137(1) GPa (McCarthy *et al.* 2008) and 134(1) GPa (Nestola *et al.* 2006). The value of the Grüneisen parameter for both the Einstein and the Debye approximation are unchanged within the estimated standard deviation on substitution of either of these revised values for the bulk modulus.

The temperature dependence of the thermodynamic Grüneisen parameter for the reduced temperature-interval $1.93 \le \vartheta_D/T \le 10.78$ has been calculated using the expression below (Barron & White 1999):

$$\gamma_{th}(T) = \frac{\alpha(T)K(T)V_m(T)}{Cv(T)} \approx \frac{\alpha(T)K_0V_m(T)}{Cp(T)}$$

where V_m is the molar volume, K_0 is the isothermal bulk modulus (assumed to be temperature-independent), α is the volume expansion coefficient, and Cv and Cp are the heat capacities at constant volume and constant pressure, respectively. For a solid at low temperature, the difference between Cv and Cp ($-TK_0\alpha^2V_m$) is small enough to be ignored; γ_{th} was calculated using the values of Cp obtained in the recent calorimetric

study of jadeite made by Hemingway *et al.* (1998), α as calculated in the Debye approximation using the fitted values from this study, and K_0 from Kandelin & Weidner (1988). The temperature dependence of γ_{th} is shown as the dashed line in Figure 5, which indicates that only a slight variation in temperature exists between 50 and 280 K, with γ_{th} varying from 0.99 at 50 K to 0.91 at 280 K. A maximum in $\gamma_{th}(T)$ occurs at approximately 110 K, where it rises to 1.16. The values of γ_{th} and γ' are physically reasonable, in quite good agreement, and they superficially appear to be close to the value of 1.06 for the ambient temperature value of γ_{th} determined in a high-temperature, high-pressure, energy-dispersive X-ray diffraction (EDXRD) study of jadeite (Zhao *et al.* 1997). However, it should be noted that the value of γ_{th} given by Zhao *et al.* is in error, and according to their quoted values of Cp, K_0, α and density, γ_{th} should in fact read 10.6, which is clearly a physically unreasonable value, probably arising from the intrinsic low resolution of the EDXRD technique. The range in values of γ_{th} calculated in this current study is in excellent agreement with that determined by X-ray diffraction for the enstatite – ferrosilite solid solution, found to be independent of composition, with values of γ_{th} in the range ~0.85–0.89 (Yang & Ghose 1994). It is also in agreement with the compressibility studies of Dietrich & Arndt (1982) on orthopyroxene of composition $(Ca_{0.01}Fe_{0.13}Mg_{0.85})SiO_3$; they found γ_{th} = 0.85, and for $MgSiO_3$, γ_{th} is 0.90 (Ostrovsky 1979). From this limited documentation, it is evident that γ_{th} in pyroxenes appears to have a significantly smaller value than other common crustal and mantle phases (Poirier 2000).

It is quite clear that the magnitudes of the Einstein and Debye temperatures derived from the low-temperature volume expansion, 369 and 539 K, respectively, are low if compared to the elastic Debye temperature based on the average velocity of sound measured at room temperature. From Poirier (2000), the elastic Debye temperature is given by:

$$\vartheta_D = 251.2\left(\frac{\rho}{M}\right)^{1/3} v_m$$

where

$$v_m = 3^{1/3}\left(\frac{1}{v_p^3}+\frac{2}{v_s^3}\right)^{-1/3}$$

ρ is the density, and M is the mean atomic mass. Using $\rho = 3.348 \times 10^3$ kg m^{-3}, $v_p = 8.78$ km s^{-1} and $v_s = 5.05$ km s^{-1} (Kandelin & Weidner 1988), the elastic Debye temperature can be estimated to be 774 K. Kieffer (1979) has discussed the discrepancy between the observed value of heat capacity and that calculated from the elastic Debye temperature in a number of papers, and has derived a sophisticated model to fit the calorimetric data. In this study, we simply show that the values of the Einstein and Debye temperatures derived from the volume expansivity are consistent with the data on heat capacity published by Hemingway *et al.* (1998).

Figure 6 shows the experimentally determined value of the heat capacity of jadeite compared with a number of calculations and fits. The dotted line shows the heat capacity calculated for a Debye model with the elastic Debye temperature of 774 K, and the dashed line shows the results of a least-squares fit to these data, for which the Debye temperature was found to be 815 K. Consideration of the figure shows that at low temperatures, the heat capacity observed is greater than either calculation, showing that jadeite has more active modes than those predicted by a Debye model. At high temperatures, the opposite effect is found, indicating that there are significantly fewer active modes than the Debye model predicts. The solid line in the figure shows the results of fitting a simple model composed of the sum of two independent specific heat contributions $Cv_i(E_i)$ with the assumption of Dulong–Petit behavior for n oscillators, and the fraction of the specific heat contribution, x, a refinable variable and $0 \le x \le 1$.

$$Cp \sim Cv = \left(xCv_1\left(\vartheta_1\right)+\left(1\text{-}x\right)Cv_2\left(\vartheta_2\right)\right)$$

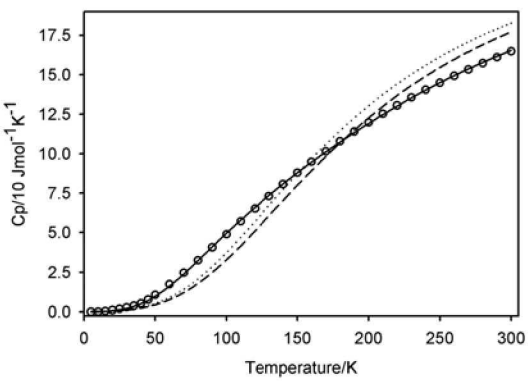

FIG. 6. The temperature dependence of the isobaric heat capacity (Hemingway *et al.* 1998) and fits to these data. The dashed line shows a least-squares fit to these data assuming a Debye model for the isochoric heat capacity, whereas the dotted line shows the expected temperature-variation for a Debye model with a characteristic temperature based on the experimentally determined speeds of sound. The full line shows the result of fitting the data on heat capacity to the sum of a Debye term and an Einstein term assuming Dulong–Petit behavior at high temperature.

where $Cv_i = 3R\left(\frac{T}{\vartheta_{D_i}}\right)^3 \int_0^{\vartheta_{D_i}/T} \frac{x^4 e^x}{\left(e^x - 1\right)^2} dx$ for a Debye model and $Cv_i = 3R\left(\frac{\vartheta_{E_i}}{T}\right)^2 \frac{e^{\vartheta_{E_i}/T}}{\left(e^{\vartheta_{E_i}/T} - 1\right)^2}$ for an Einstein model.

The figure shows that over the temperature range of interest, the fit to the data using a sum of an Einstein heat capacity with ϑ_1 = 1030 K and a Debye heat capacity with ϑ_2 = 511 K and x = 0.44 is excellent. An equally good fit was found to the sum of two Einstein oscillators with ϑ_1 = 920 K, ϑ_2 = 315 K and x = 0.57. The fit to two independent Debye heat capacities was found to be significantly poorer. There is consistency between the Debye temperatures derived from the volume expansion and the heat capacity data, the agreement between the lower Einstein temperature in the two Einstein oscillator model and that determined from the unit-cell volume expansion is, however, less good. Despite this, there is qualitative agreement between these temperatures and modes observed by vibrational spectroscopy. A Debye temperature of 511 K corresponds to a frequency of 355 cm^{-1}, which is within the range predicted for lattice modes in pyroxenes (Shurvell *et al.* 2001); an Einstein temperature of 1030 K, with corresponding frequency 716 cm^{-1}, is very close to the frequency of the Si–O–Si stretch in jadeite of 705 cm^{-1}, measured by Ohashi & Sekita (1982) using Raman spectroscopy. A more detailed comparison would require full assignments of modes in the vibrational spectra and the measurement of the vibrational density of states function for jadeite, neither of which have been made yet.

Crystal-Structure Refinement

To allow rapid data-collection times, of the order of 75 minutes per temperature, with good estimated standard deviations on all structural variables, it was necessary to refine two separate banks of data from POLARIS simultaneously. The CCSL-based software used for the lattice-parameter extraction of the HRPD data was not capable of carrying out multi-bank refinement, and hence the Rietveld refinement was undertaken using the GSAS suite of programs (Larson & Von Dreele 1988). The lineshape used in the refinements was profile function 3, a pseudo-Voigt convoluted with two back-to-back exponentials, and is therefore different from that used in the CCSL software. These differences in peak parameterization, flight-path uncertainties and resolution of the two instruments are sufficient to result in differences in lattice constants far in excess of their estimated standard deviations. To ensure consistency between the lattice parameters collected on the two instruments, therefore, the HRPD results were used to calibrate those from POLARIS. To achieve this, the sample-temperature log for each POLARIS run was integrated to determine the mean temperature experienced by the sample during the data collection. The lattice parameters for that particular temperature were determined by calculation using the parameterization of the HRPD results with estimated standard deviations set to those derived from HRPD cell and intensity least-squares refinement. The primary flight-paths for the two detector banks from POLARIS were then introduced as additional least-squares variables in the refinement rather than the lattice parameters. The average fractional variation of both flight paths ($\Delta L/L$) for the whole range in temperature was less than the estimated standard deviations of the lattice parameters for a single HRPD measurement. Furthermore, to ensure that the estimated standard deviations of the unit cell were not underestimated using this method, once convergence of the Rietveld refinement had been achieved, the flight paths were set and fixed at instrument-calibration values and the refinement repeated. For all temperatures, the estimated standard deviations of the lattice parameters derived from this analysis were less than those being applied from the HRPD results, indicating, if anything, that the applied errors were overestimates. The structural parameters showed no significant changes between these two refinement modes.

The 2.5 K data were refined first, with the converged results being used as a seed for the subsequent temperature, this procedure being carried out iteratively until the final-temperature dataset was processed. The starting structural coordinates were derived from the ambient-temperature structure of jadeite (Cameron *et al.* 1973), with appropriate isotropic displacement parameters taken from the 10 K single-crystal, neutron-diffraction study of diopside (Prencipe *et al.* 2000). For the 2.5 K datasets, convergence from these starting parameters was rapid, resulting in χ^2 = 6.2, Rwp = 0.021, Rp = 0.036 for 50 variables. Attempts to refine the anions anisotropically were unsuccessful at low temperatures, always leading to non-positive-definite atomic displacement parameters, even at temperatures greater than 200 K, the change in χ^2 for an anisotropic model over an isotropic model was not statistically meaningful. The isotropic model was therefore retained for all temperatures. Owing to the compact, polycrystalline nature of the source material, it was not necessary to refine either a preferred orientation correction or an extinction parameter for any of these data. This is in marked contrast to the structural refinement of powder samples of other clinopyroxenes derived from large single crystals where the perfect cleavage gives rise to acicular particles with a high degree of crystallographic perfection. Agreement factors were found to show little variation among datasets from different temperatures, indicating that there were no additional systematic temperature-dependent effects that were not being accounted for in the refinements. The refinement details are shown in Table 3, with the structural

parameters listed in Table 4. A typical fit to the two datasets is shown in Figure 7, in this case for the data collected at 2.5 K.

Oxygen packing

In an O-rotated clinopyroxene *C*2/*c* structure, the arrangement of oxygen atoms is close to being cubic close-packed (Thompson 1970). A measure of the deviation from this configuration has recently been proposed by Hattori *et al.* (2000) using the average of the sums of the root squares of the displacements of the anion array from the ideal close-packed coordinates. Hattori *et al.* proposed three separate deviation parameters, D_{total}, related to the total displacement, $D_{//a^*}$, related to the displacement along the stacking direction, and D_{b-c}, related to the displacement within the stacking layer.

$$D_{total} = \frac{1}{3}\sum_{i=1}^{3}\sqrt{(a\Delta x_i)^2 + (b\Delta y_i)^2 + (c\Delta z_i)^2}$$

$$D_{//a^*} = \frac{1}{3}\sum_{i=1}^{3}\sqrt{(a\Delta x_i)^2}$$

$$D_{b\text{-}c} = \frac{1}{3}\sum_{i=1}^{3}\sqrt{(b\Delta y_i)^2 + (c\Delta z_i)^2}$$

The temperature dependence of the three distortion parameters was found to be linear throughout the whole temperature-interval, with the dominant distortion being the displacement within the stacking layer, as illustrated by Figure 8. In contrast to the high-pressure results on $FeGeO_3$ clinopyroxene, where increasing pressure decreased the deviation parameters (Hattori *et al.* 2000), the effect of increasing temperature in jadeite is to increase the deviation parameters, *i.e.*, to distort the structure further away from ideality. Analysis of the high-temperature data of Cameron *et al.* (1973) shows identical trends in the deviation parameters to those we have determined at low temperature, albeit with different gradients but similar magnitudes.

TABLE 3. INSTRUMENTAL AND REFINEMENT DETAILS FOR DATA COLLECTED USING THE POLARIS DIFFRACTOMETER

Instrumental details	
Diffractometer	POLARIS (neutron time-of-flight powder diffractometer)
Detectors Bank 1	216 ZnS scintillation
Mean Bragg angle	90° 2θ
Flight path	~12.8 m
Data range	2.0 – 19.0 ms
Time channel binning	$\Delta t/t = 5 \times 10^{-4}$
Observations	4395
Detectors Bank 2	58 ^{3}He gas tubes
Mean Bragg angle	145° 2θ
Flight path	~12.8 m
Data range	2.0 – 19.5ms
Time channel binning	$\Delta t/t = 5 \times 10^{-4}$
Observations	4565
Refinement details	
Space group	*C*2/*c*
Z	4
Unit-cell refinement	calibrated to HRPD parameterization
Refined parameters	
Structural	20 (14 coordinates, 6 atomic displacement parameters)
Profile	2 per bank
Background	10 Chebychev polynomials of the first kind per bank
Flight paths	2 per bank (DIFC and DIFA)
Displacement param.	all atoms isotropic
Agreement factors	$\chi^2 = [R_{wp} / R_{exp}]^2$; see Table 4

Atomic displacement parameters

Classical, rigid-ion lattice-dynamics calculations extended to the whole Brillouin zone has been carried out on diopside, with the results suggesting a significant zero-point motion contribution to the atomic displacement parameters at room temperature (Pilati *et al.* 1996). Experimental verification of this prediction was made in a single-crystal neutron-diffraction study of diopside at 10 K, where, on average, the zero-point displacement contributed 35% of the room-temperature values (Prencipe *et al.* 2000). In particular, the Ca cation was found to show a significantly larger isotropic displacement parameter than the other cations, reflecting the more relaxed polyhedron environment for the *M*2 cation in clinopyroxenes. A similar observation at temperatures of the order of 4.2 K has been found for the Li ion in spodumene, the Ca ions in hedenbergite ($Hd_{80}Fs_{13}Di_7$) and diopside ($Di_{87}Hd_{13}$), the Co in the *M*2 site of $CoGeO_3$, and the Na ions in aegirine, $NaFeGe_2O_6$ (K.S. Knight, unpubl. data in all cases) and jadeite (this work).

Figure 9 shows the isotropic displacement parameters for jadeite between 2.4 and 268 K. All atoms show the expected dependence on temperature, a saturation at low temperatures, *i.e.*, the zero-point displacements, and the development of a more linear behavior at higher temperatures (Willis & Pryor 1975). For the cations, the relationship Na U_{iso} > Al U_{iso} > Si U_{iso} holds for all temperatures measured, with the percentage contribution of the zero-point displacements to the 268 K displacements being 46% for Na, 55% for Al and 55% for Si. The magnitude of the zero-point displacement for Na is approximately three times greater than those of Al and Si. For the anions, the behavior is more subtle, and for all temperatures measured, O2 U_{iso} exceeds O1 U_{iso} and O3 U_{iso}. The zero-point displacements of O2 and O1 are approximately equal, whereas that for O3 is slightly smaller. The temperature dependencies of the displacement parameters of O2 and O3 are such that O1 U_{iso} exceeds O3 U_{iso} up to ~175 K, at which point this trend reverses. The increase in O3 U_{iso} at this temperature may be related to the dominant structural distortion within the chain of tetrahedra, which is the increase in the O3 – O3 edge length beginning at temperatures of the order of 100 K.

We have demonstrated earlier that the volume expansion of jadeite could be successfully parameterized in terms of a Debye internal energy function, and for a Debye solid, the variation of the isotropic displacement with temperature parameters has the form (James 1962)

$$\overline{u^2(T)} = \frac{3h^2T}{4\pi^2 M k_B \vartheta_D^2}\left[\phi\left(\frac{\vartheta_D}{T}\right)+\frac{\vartheta_D}{4T}\right]$$

where M is the mass of the vibrating species, h is Planck's constant, and the function $\phi(\vartheta_D/T)$ is given by

$$\phi\left(\frac{\vartheta_D}{T}\right) = \left(\frac{T}{\vartheta_D}\right)\int_0^{\vartheta_D/T}\frac{x\,dx}{e^x-1}$$

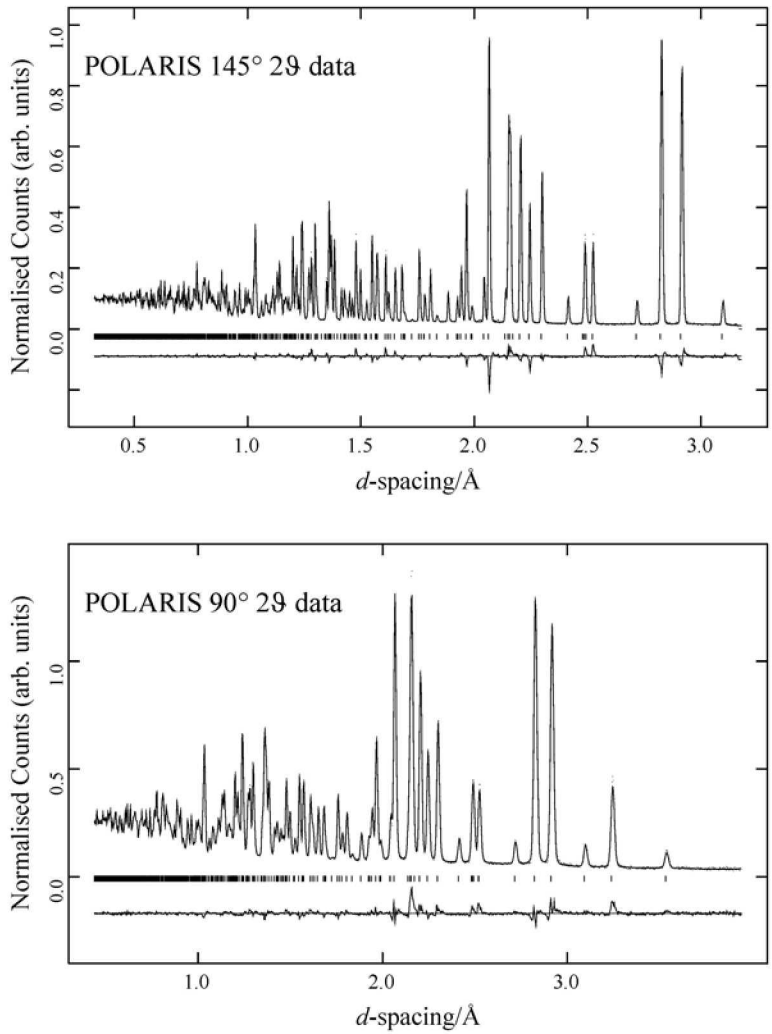

FIG. 7. Rietveld refinements of powder neutron-diffraction data for jadeite collected at 2.5 K for the two banks of POLARIS data. Observed data are points, calculated data are shown by the full line. In these cases, the difference plots are simply observed intensity minus calculated intensity.

TABLE 4. STRUCTURAL PARAMETERS FOR JADEITE BETWEEN 2.4 AND 259 K

Temp.	*a*, Å	*b*, Å	*c*, Å	β, °	Na *y*	Na *U*iso, Å^2	Al *y*	Al *U*iso, Å^2	Si *x*	Si *y*	Si *z*	Si *U*iso, Å^2
2.4	9.41591(9)	8.55521(4)	5.22073(20)	107.5641(7)	0.3012(1)	0.0049(1)	0.9070(1)	0.0016(1)	0.29103(5)	0.09346(6)	0.22808(9)	0.00138(6)
10.3	9.41591(9)	5.22073(4)	5.22073(20)	107.5641(7)	0.3010(1)	0.0050(1)	0.9070(1)	0.0017(1)	0.29097(5)	0.09342(6)	0.22806(9)	0.00138(6)
19.7	9.41591(9)	8.55521(4)	5.22073(20)	107.5641(7)	0.3011(1)	0.0049(1)	0.9070(1)	0.0016(1)	0.29103(5)	0.09349(6)	0.22815(9)	0.00137(6)
29.5	9.41591(9)	8.55521(4)	5.22073(20)	107.5642(7)	0.3011(1)	0.0049(1)	0.9070(1)	0.0016(1)	0.29102(5)	0.09347(6)	0.22813(9)	0.00137(6)
39.0	9.41591(9)	8.55521(4)	5.22073(20)	107.5645(7)	0.3011(1)	0.0051(1)	0.9070(1)	0.0015(1)	0.29106(5)	0.09347(6)	0.22806(9)	0.00138(6)
47.5	9.41592(9)	8.55523(4)	5.22073(20)	107.5650(7)	0.3011(1)	0.0051(1)	0.9070(1)	0.0016(1)	0.29104(5)	0.09350(6)	0.22813(9)	0.00141(6)
55.1	9.41594(9)	8.55527(4)	5.22074(20)	107.5655(7)	0.3012(1)	0.0053(1)	0.9069(1)	0.0016(1)	0.29107(5)	0.09349(6)	0.22808(9)	0.00144(6)
64.0	9.41599(9)	8.55535(4)	5.22075(20)	107.5662(7)	0.3011(1)	0.0055(1)	0.9071(1)	0.0017(1)	0.29104(5)	0.09349(6)	0.2281(1)	0.00150(7)
73.4	9.41607(9)	8.55547(4)	5.22077(20)	107.5670(7)	0.3010(1)	0.0055(1)	0.9071(1)	0.0016(1)	0.29105(5)	0.09342(6)	0.2281(1)	0.00145(7)
83.0	9.41620(9)	8.55566(4)	5.22080(20)	107.5677(7)	0.3011(1)	0.0057(1)	0.9069(1)	0.0018(1)	0.29104(5)	0.09344(6)	0.2281(1)	0.00149(7)
96.5	9.41644(9)	8.55600(4)	5.22088(20)	107.5686(7)	0.3012(1)	0.0059(1)	0.9070(1)	0.0018(1)	0.29100(5)	0.09347(6)	0.22805(9)	0.00153(6)
106.4	9.41666(9)	8.55631(4)	5.22095(20)	107.5692(7)	0.3011(1)	0.0061(1)	0.9069(1)	0.0019(1)	0.29103(6)	0.09340(6)	0.2281(1)	0.00168(7)
114.5	9.41686(9)	8.55660(4)	5.22101(20)	107.5695(7)	0.3012(1)	0.0065(1)	0.9068(1)	0.0020(1)	0.29105(6)	0.09342(6)	0.2280(1)	0.00166(7)
121.9	9.41707(9)	8.55688(4)	5.22108(20)	107.5698(7)	0.3012(1)	0.0065(1)	0.9069(1)	0.0020(1)	0.29093(6)	0.09341(6)	0.2279(1)	0.00162(7)
138.8	9.41759(9)	8.55760(4)	5.22127(20)	107.5703(7)	0.3011(1)	0.0071(1)	0.9069(1)	0.0024(1)	0.29098(5)	0.09341(6)	0.2280(1)	0.00185(7)
149.6	9.41797(9)	8.55811(4)	5.22140(20)	107.5705(7)	0.3010(1)	0.0073(1)	0.9070(1)	0.0023(1)	0.29099(5)	0.09346(6)	0.2280(1)	0.00177(7)
156.8	9.41823(9)	8.55846(4)	5.22150(20)	107.5706(7)	0.3012(1)	0.0073(1)	0.9070(1)	0.0024(1)	0.29096(5)	0.09347(6)	0.2280(1)	0.00181(6)
165.9	9.41857(9)	8.55892(4)	5.22162(20)	107.5707(7)	0.3011(1)	0.0076(1)	0.9068(1)	0.0024(1)	0.29100(6)	0.09349(6)	0.2279(1)	0.00191(7)
175.1	9.41893(9)	8.55941(4)	5.22176(20)	107.5708(7)	0.3011(1)	0.0078(2)	0.9068(1)	0.0025(1)	0.29094(5)	0.09343(6)	0.2279(1)	0.00191(7)
184.5	9.41931(9)	8.55991(4)	5.22190(20)	107.5708(7)	0.3010(1)	0.0082(2)	0.9067(1)	0.0027(1)	0.29099(5)	0.09339(6)	0.2279(1)	0.00200(7)
194.3	9.41972(9)	8.56046(4)	5.22206(20)	107.5709(7)	0.3010(1)	0.0083(2)	0.9069(1)	0.0027(1)	0.29099(6)	0.09335(6)	0.2279(1)	0.00202(7)
203.6	9.42012(9)	8.56099(4)	5.22221(20)	107.5709(7)	0.3012(1)	0.0087(2)	0.9067(1)	0.0028(1)	0.29093(6)	0.09338(6)	0.2279(1)	0.00206(7)
213.2	9.42054(9)	8.56154(4)	5.22237(20)	107.5710(7)	0.3011(1)	0.0089(2)	0.9067(1)	0.0028(1)	0.29099(6)	0.09334(6)	0.2278(1)	0.00210(7)
222.4	9.42095(9)	8.56209(4)	5.22253(20)	107.5710(7)	0.3011(1)	0.0094(2)	0.9066(1)	0.0030(1)	0.29092(6)	0.09334(6)	0.2278(1)	0.00221(7)
231.6	9.42137(9)	8.56264(4)	5.22269(20)	107.5710(7)	0.3012(1)	0.0095(2)	0.9067(1)	0.0030(1)	0.29097(6)	0.09333(6)	0.2278(1)	0.00216(7)
240.6	9.42179(9)	8.56318(4)	5.22285(20)	107.5710(7)	0.3011(1)	0.0099(2)	0.9066(1)	0.0032(1)	0.29086(6)	0.09329(6)	0.2278(1)	0.00225(7)
249.8	9.42222(9)	8.56375(4)	5.22302(20)	107.5710(7)	0.3011(1)	0.0101(2)	0.9066(1)	0.0032(1)	0.29088(6)	0.09331(6)	0.2278(1)	0.00229(7)
259.1	9.42266(9)	8.56432(4)	5.22320(20)	107.5710(7)	0.3011(1)	0.0105(2)	0.9064(1)	0.0034(1)	0.29090(6)	0.09329(6)	0.2276(1)	0.00236(7)
268.3	9.42310(9)	8.56490(4)	5.22337(20)	107.5710(7)	0.3012(1)	0.0106(2)	0.9065(1)	0.0034(1)	0.29090(6)	0.09329(6)	0.2276(1)	0.00249(8)

TABLE 4 (cont'd). STRUCTURAL PARAMETERS FOR JADEITE BETWEEN 2.4 AND 259 K

Temp.	O1 *x*	O1 *y*	O1 *z*	O1 *U*iso, Å^2	O2 *x*	O2 *y*	O2 *z*	O2 *U*iso, Å^2	O3 *x*	O3 *y*	O3 *z*	O3 *U*iso, Å^2	χ^2
2.4	0.10923(4)	0.07611(4)	0.12852(7)	0.00316(5)	0.36083(4)	0.26339(4)	0.29370(8)	0.00321(5)	0.35379(4)	0.00773(4)	0.00611(8)	0.00295(5)	6.21
10.3	0.10921(4)	0.07611(5)	0.12841(7)	0.00315(5)	0.36088(4)	0.26341(4)	0.29378(8)	0.00316(5)	0.35376(5)	0.00772(4)	0.00612(8)	0.00292(5)	3.35
19.7	0.10920(4)	0.07611(4)	0.12849(7)	0.00313(5)	0.36083(4)	0.26342(4)	0.29370(8)	0.00315(6)	0.35380(5)	0.00774(4)	0.00609(8)	0.00297(5)	3.40
29.5	0.10924(4)	0.07613(5)	0.12851(7)	0.00316(5)	0.36087(4)	0.26339(4)	0.29367(8)	0.00318(6)	0.35382(5)	0.00769(4)	0.00613(8)	0.00298(5)	3.39
39.0	0.10923(4)	0.07614(5)	0.12844(7)	0.00326(5)	0.36087(4)	0.26340(4)	0.29370(8)	0.00320(6)	0.35381(5)	0.00772(4)	0.00618(8)	0.00299(5)	3.39
47.5	0.10922(4)	0.07613(5)	0.12848(7)	0.00326(5)	0.36088(4)	0.26342(4)	0.29375(8)	0.00322(6)	0.35377(5)	0.00772(4)	0.00608(8)	0.00300(5)	3.38
55.1	0.10921(4)	0.07614(5)	0.12844(7)	0.00324(5)	0.36084(4)	0.26335(4)	0.29368(8)	0.00327(6)	0.35374(5)	0.00771(4)	0.00615(8)	0.00307(5)	3.35
64.0	0.10923(4)	0.07612(5)	0.12847(7)	0.00342(5)	0.36083(4)	0.26338(4)	0.29368(8)	0.00341(6)	0.35377(5)	0.00771(4)	0.00616(8)	0.00319(5)	3.40
73.4	0.10922(4)	0.07609(5)	0.12840(7)	0.00329(5)	0.36086(4)	0.26339(4)	0.29370(8)	0.00339(6)	0.35382(5)	0.00769(4)	0.00614(8)	0.00318(5)	3.32
83.0	0.10921(4)	0.07608(5)	0.12844(7)	0.00331(5)	0.36087(4)	0.26338(4)	0.29363(8)	0.00337(6)	0.35379(5)	0.00767(4)	0.00617(8)	0.00316(5)	3.38
96.5	0.10919(4)	0.07607(5)	0.12845(7)	0.00336(6)	0.36083(4)	0.26338(4)	0.29356(8)	0.00349(6)	0.35378(5)	0.00768(4)	0.00615(8)	0.00322(5)	3.28
106.4	0.10919(4)	0.07605(5)	0.12837(8)	0.00352(5)	0.36084(5)	0.26335(4)	0.29361(9)	0.00366(6)	0.35380(5)	0.00765(4)	0.00616(8)	0.00338(5)	3.61
114.5	0.10915(4)	0.07600(5)	0.12841(7)	0.00351(6)	0.36079(5)	0.26335(4)	0.29355(9)	0.00370(6)	0.35381(5)	0.00760(4)	0.00613(8)	0.00343(5)	3.39
121.9	0.10916(4)	0.07604(5)	0.12830(8)	0.00357(6)	0.36083(5)	0.26330(4)	0.29353(9)	0.00373(5)	0.35377(5)	0.00767(4)	0.00619(8)	0.00350(6)	3.36
138.8	0.10919(4)	0.07602(5)	0.12832(7)	0.00378(6)	0.36077(4)	0.26333(4)	0.29332(8)	0.00399(6)	0.35385(5)	0.00759(4)	0.00626(8)	0.00477(5)	3.13
149.6	0.10923(4)	0.07600(5)	0.12836(7)	0.00374(6)	0.36080(4)	0.26332(4)	0.29341(8)	0.00397(6)	0.35380(5)	0.00760(4)	0.00623(8)	0.00369(5)	3.08
156.8	0.10920(4)	0.07605(5)	0.12834(7)	0.00380(6)	0.36080(4)	0.26328(4)	0.29337(8)	0.00407(6)	0.35378(5)	0.00760(4)	0.00618(8)	0.00381(6)	3.12
165.9	0.10922(4)	0.07602(5)	0.12840(8)	0.00371(6)	0.36077(5)	0.26332(4)	0.29337(9)	0.00407(6)	0.35384(5)	0.00755(4)	0.00617(8)	0.00378(6)	3.17
175.1	0.10923(4)	0.07599(5)	0.12830(7)	0.00399(6)	0.36082(5)	0.26324(4)	0.29324(9)	0.00424(6)	0.35379(5)	0.00759(4)	0.00619(8)	0.00393(6)	3.06
184.5	0.10917(4)	0.07598(5)	0.12826(7)	0.00400(6)	0.36083(5)	0.26323(4)	0.29324(9)	0.00435(6)	0.35375(5)	0.00760(4)	0.00622(8)	0.00406(6)	3.05
194.3	0.10925(4)	0.07592(5)	0.12829(8)	0.00400(6)	0.36078(5)	0.26321(4)	0.29318(9)	0.00435(6)	0.35374(5)	0.00756(4)	0.00624(9)	0.00409(6)	3.22
203.6	0.10913(4)	0.07591(5)	0.12817(8)	0.00414(6)	0.36077(5)	0.26320(4)	0.29312(9)	0.00463(6)	0.35379(5)	0.00750(4)	0.00621(9)	0.00428(6)	3.07
213.2	0.10918(4)	0.07595(5)	0.12820(8)	0.00419(6)	0.36077(5)	0.26323(4)	0.29310(9)	0.00462(6)	0.35381(5)	0.00753(4)	0.00619(9)	0.00427(6)	3.14
222.4	0.10917(4)	0.07594(5)	0.12831(8)	0.00425(6)	0.36077(5)	0.26321(4)	0.29311(9)	0.00425(6)	0.35375(5)	0.00753(5)	0.00611(9)	0.00450(6)	3.11
231.6	0.10914(4)	0.07584(5)	0.12815(8)	0.00430(6)	0.36079(5)	0.26313(4)	0.29306(9)	0.00500(7)	0.35370(5)	0.00750(5)	0.00604(9)	0.00463(6)	3.21
240.6	0.10918(4)	0.07600(5)	0.12821(8)	0.00448(6)	0.36076(5)	0.26317(4)	0.29302(9)	0.00509(6)	0.35375(5)	0.00752(5)	0.00612(9)	0.00473(6)	3.11
249.8	0.10916(4)	0.07590(5)	0.12815(8)	0.00454(6)	0.36079(5)	0.26311(4)	0.29295(9)	0.00514(7)	0.35368(5)	0.00745(5)	0.00608(9)	0.00483(6)	3.11
259.1	0.10917(5)	0.07588(5)	0.12812(8)	0.00458(6)	0.36077(5)	0.26311(4)	0.29296(9)	0.00534(7)	0.35368(5)	0.00755(5)	0.00611(9)	0.00491(6)	3.10
268.3	0.10914(5)	0.07591(5)	0.12808(8)	0.00478(6)	0.36073(5)	0.26312(4)	0.29288(9)	0.00548(7)	0.35367(5)	0.00747(5)	0.00607(9)	0.00499(6)	3.11

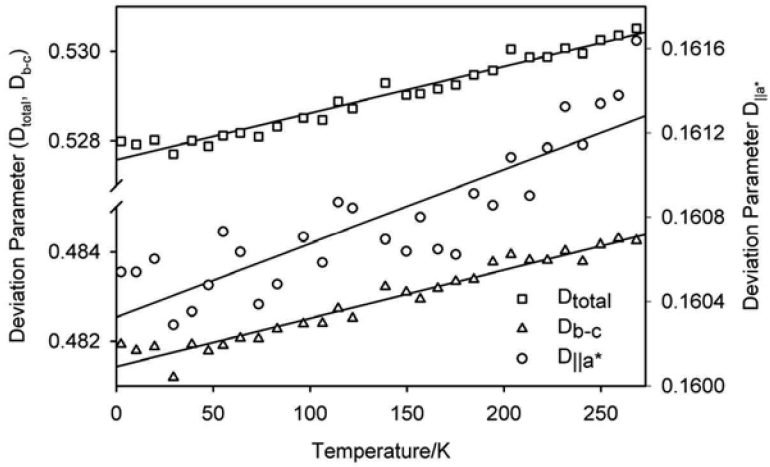

FIG. 8. The variation with temperature of the three Hattori distortion parameters (Hattori *et al.* 2000) for jadeite.

It should be noted that this temperature variation is a single-parameter fit in ϑ_D, and hence it not only requires data to be corrected for all systematic errors to be truly assessed, it also probably applies too great a constraint on the zero-point displacement in anything other than structurally simple materials for which it was originally derived. Indeed this was found to be the case in jadeite, in which attempts to fit any of the individual atomic displacement parameters to this expression were generally unsuccessful. However, allowing the zero-point displacement to be an additional variable in the fitting procedure, whilst retaining the temperature dependence implicit within the Debye function, *i.e.*, using the expression below,

$$\overline{u^2}(T) = \frac{3h^2T}{4\pi^2 M k_B \vartheta_D^2}\phi\left(\frac{\vartheta_D}{T}\right)+A$$

resulted in the excellent fits to the data, shown as solid lines in the figure.

The effective vibrational Debye temperatures for the displacements of the individual atoms, determined by weighted least-squares, are Na 442(3) K, Al 650(9) K, Si 791(11) K, O1 855(7) K, O2 739(5) K and O3 764(4) K. The fitted zero-point displacements, A, are: Na 4.87(4) $\times 10^{-3}$ Å^2, Al 1.57(3) $\times 10^{-3}$ Å^2, Si 1.39(2) $\times 10^{-3}$ Å^2, O1 3.18(2) $\times 10^{-3}$ Å^2, O2 3.17(2) $\times 10^{-3}$ Å^2 and O3 2.96(1) $\times 10^{-3}$ Å^2. Assuming the Debye temperatures from the fitting procedure are correct, the calculated zero-point displacements are: Na 3.58 $\times 10^{-3}$ Å^2, Al 2.07 $\times 10^{-3}$ Å^2, Si 1.64 $\times 10^{-3}$ Å^2, O1 2.66 $\times 10^{-3}$ Å^2, O2 3.08 $\times 10^{-3}$ Å^2 and O3 2.98 $\times 10^{-3}$ Å^2. The zero-point displacements of anions are in fairly good agreement with the free refinement, but the cations show significant differences from those expected for a simple Debye solid. Both the lower vibrational Debye temperature and higher zero-point displacement for Na reflect the softness of the NaO_8 square antiprismatic polyhedron compared to the increasing rigidities of the AlO_6 octahedral polyhedron and the SiO_4 tetrahedral polyhedron.

The NaO_8 square antiprism

Figure 10 shows the NaO_8 polyhedron for jadeite labeled according to the recommended nomenclature for clinopyroxene structures of Burnham *et al.* (1967). Four of the eight coordinating oxygen atoms, O3C1,2, O3D1,2, are shared with the chains of silicate tetrahedra and four are shared with the AlO_6 octahedron, O1A1, O1B1, O2C2 and O2D2. The sodic clinopyroxenes are characterized by two long Na–O bonds at ~2.7 Å (Na–O3C2 and –O3D2), which link adjacent bands of octahedra, and six shorter Na–O bonds in the range 2.3–2.4 Å. Viewed down the **c** axis, the coordination polyhedra can be seen to be highly distorted square antiprism.

The effect of temperature on the *M*2 site in clinopyroxenes is complex, with evidence of a change in coordination number from 8 to 6 in the calcic clinopyroxenes diopside and hedenbergite at high temperatures (Cameron *et al.* 1973). In contrast, the high-temperature study of Cameron *et al.* (1973) showed jadeite to remain 8-fold-coordinated from 297 to 1073 K, and hence the NaO_8 polyhedron in jadeite can be treated in a simple manner using the conventional distortion parameters of quadratic elongation and bond-angle variance (Robinson *et al.* 1971). A regular square antiprism is

characterized by the ratio of its volume to the cube of the center-vertex distance of $(16\sqrt{2}+16)/[3(2\sqrt{2}+1)^{3/2}]$ and has two inter center–vertex distance 'bond' angles of $\cos^{-1}[-3/(2\sqrt{2}+1)]$, ~141.59°, and $\cos^{-1}[1/(2\sqrt{2}+1)]$, ~74.86°. In this work, the square antiprism angle variance has been calculated using the larger of the two angles as the reference angle, the quadratic elongation was calculated in the standard manner. At 2.5 K, the quadratic elongation is 1.0377, and the square antiprism angle variance is 408.28 degrees squared, the magnitudes of both reflecting the significant distortion from ideality of this polyhedron.

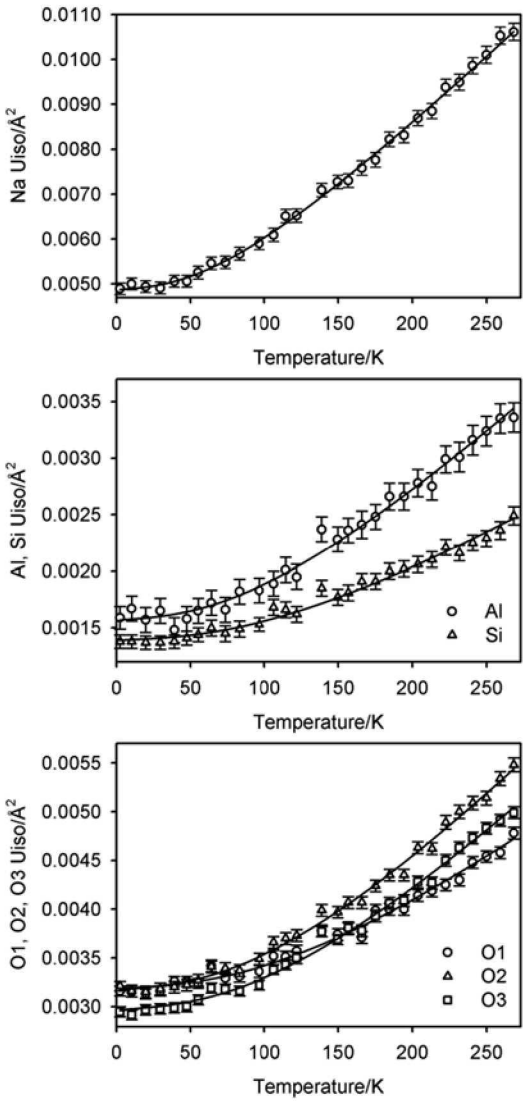

FIG. 9. The temperature dependence of the isotropic atomic displacement parameters for jadeite and the results of least-squares fits to a modified Debye model. All data show the large fraction of the contribution to the zero-point motion at the ambient temperature value. The large magnitude of the *M*2 (Na) isotropic atomic displacement parameter appears to be universal for clinopyroxenes irrespective of coordination number.

The volume of the NaO_8 polyhedron shows a significant variation with temperature, changing from a saturated value of 24.53 Å^3 at 2.5 K to 24.63 Å^3 at 268 K, with the volume moving away from the saturated value at temperatures of the order of 80–100 K. Figure 11 shows the polyhedron volume and an unweighted fit to the data using an identical expression to that used for fitting the unit-cell edges. The fitted value of the energy corresponds to a characteristic frequency of 237 cm^{-1}, which is close to the observed bands of 203, 221 and 255 cm^{-1} in the Raman spectrum of jadeite (Smith & Gendron 1997), and is of the correct order of magnitude for some of the *M*2 mode assignments in diopside (Tomisaka & Iishi 1980). From the fitted results, the high-temperature volume-expansion coefficient for the NaO_8 square antiprism is estimated at 2.9×10^{-5} K^{-1}, whereas Cameron *et al.* (1973) determined 3.7×10^{-5} K^{-1} from their high-temperature data. Despite this relatively large change in volume at low temperatures, it is not accompanied by significant distortion of polyhedra with changes in either the angle variance or the quadratic elongation, only showing weak tendencies to increase with increasing temperature. The high-temperature results of Cameron *et al.* (1973) showed that all four of the symmetry-independent Na–O bond distances increase with increasing temperature; by comparison, at low temperature, only Na–O1A1, Na–O2C2 and Na–O3C2 increase with increasing temperature, with

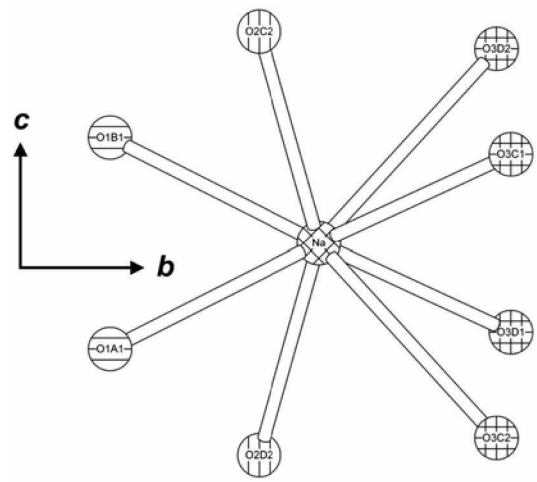

FIG. 10. The square antiprismatic coordination of sodium in jadeite, labeled according to the nomenclature of Burnham *et al.* (1967).

Na–O3C1 being independent of temperature, as shown in Figure 12. The order of fractional change in bond length with temperature shows that the bonds to the oxygen atoms shared with the chains of tetrahedra expanded significantly less than those to anions shared with the octahedra. The ratio of the Na–O1C1 distance to the Na–O3C1 distance is essentially constant throughout the whole interval of temperature, showing that at these temperatures, the Na atom does not move significantly away from the strip of octahedra, as had been observed at high temperatures (Cameron *et al.* 1973). The displacement of the sodium from the center of the coordination polyhedron is found to be independent of temperature, with an average magnitude of 0.23 Å. The bond angles within the NaO_8 polyhedron show little variation with temperature; O1A1–Na–O3D1, O2C2–Na–O2D2, O2C2–Na–O3D1, O2C2–Na–O3C2 and O3C2–Na–O3D2 all decrease, whereas O1A1–Na–O3C1, O1A1–Na–O3D2 are temperature-insensitive. Only O2C2–Na–O2D2 increases with increasing temperature.The bond lengths and selected bond-angles for the NaO_8 square antiprism are listed in Tables 5 and 6, respectively.

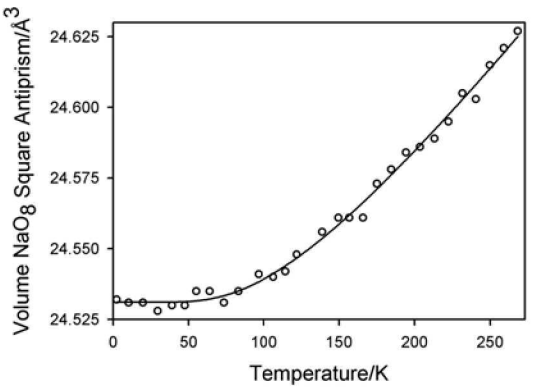

FIG. 11. The temperature dependence of the NaO_8 square antiprism in jadeite. The full line shows a fit to these data assuming an Einstein model.

The AlO_6 octahedron

The volume of the AlO_6 octahedron shows a similar but significantly smaller variation with temperature

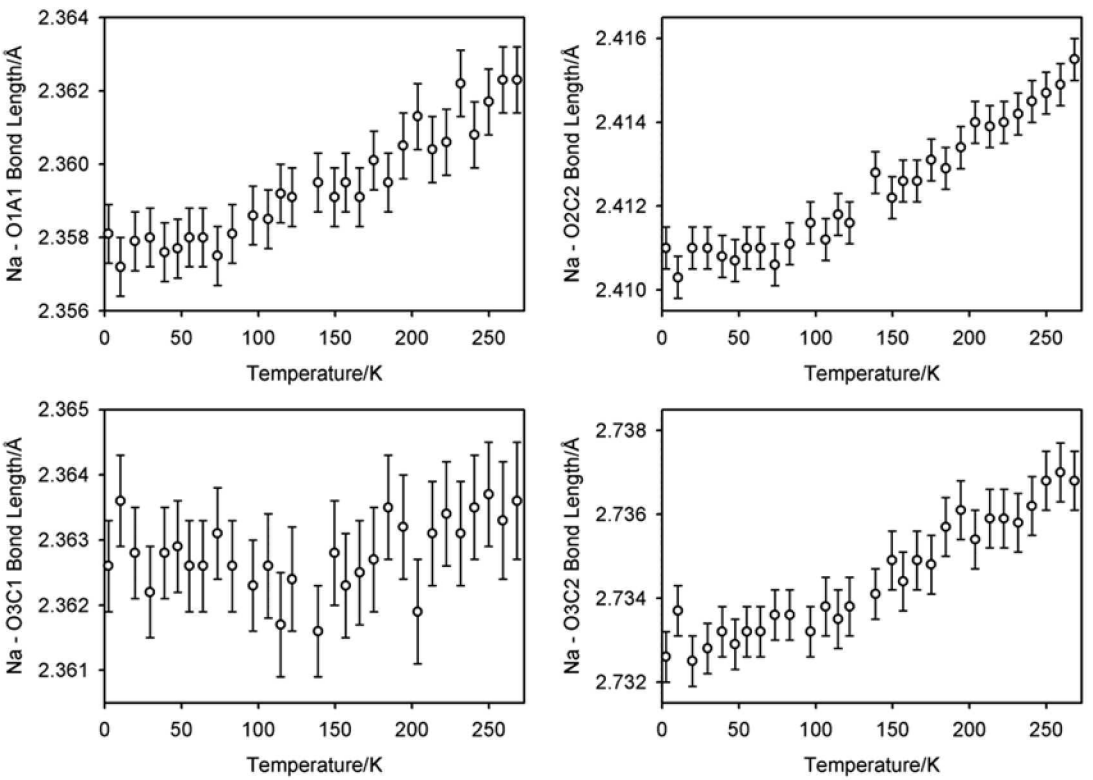

FIG. 12. The temperature dependence of the four independent Na–O bond lengths in jadeite.

TABLE 5. SELECTED BOND-LENGTHS (Å) AT THE SQUARE ANTIPRISMATIC SITE OF NaO_8 AS A FUNCTION OF TEMPERATURE (K)

Temp.	Na – O1A1	Na – O2C2	Na – O3C1	Na – O3C2
2.4	2.3581(8)	2.4110(5)	2.3626(7)	2.7326(6)
10.3	2.3572(8)	2.4103(5)	2.3636(7)	2.7337(6)
19.7	2.3579(8)	2.4110(5)	2.3628(7)	2.7325(6)
29.5	2.3580(8)	2.4110(5)	2.3622(7)	2.7328(6)
39.0	2.3576(8)	2.4108(5)	2.3628(7)	2.7332(6)
47.5	2.3577(8)	2.4107(5)	2.3629(7)	2.7329(6)
55.1	2.3580(8)	2.4110(5)	2.3626(7)	2.7332(6)
64.0	2.3580(8)	2.4110(5)	2.3626(7)	2.7332(6)
73.4	2.3575(8)	2.4106(5)	2.3631(7)	2.7336(6)
83.0	2.3581(8)	2.4111(5)	2.3626(7)	2.7336(6)
96.5	2.3586(8)	2.4116(5)	2.3623(7)	2.7332(6)
106.4	2.3585(8)	2.4112(5)	2.3626(8)	2.7338(7)
114.5	2.3592(8)	2.4118(5)	2.3617(8)	2.7335(7)
121.9	2.3591(8)	2.4116(5)	2.3624(8)	2.7338(7)
138.8	2.3595(8)	2.4128(5)	2.3616(7)	2.7341(6)
149.6	2.3591(8)	2.4122(5)	2.3628(8)	2.7349(7)
156.8	2.3595(8)	2.4126(5)	2.3623(8)	2.7344(7)
165.9	2.3591(8)	2.4126(5)	2.3625(8)	2.7349(7)
175.1	2.3601(8)	2.4131(5)	2.3627(8)	2.7348(7)
184.5	2.3595(8)	2.4129(5)	2.3635(8)	2.7357(7)
194.3	2.3605(9)	2.4134(5)	2.3632(8)	2.7361(7)
203.6	2.3613(9)	2.4140(5)	2.3619(8)	2.7354(7)
213.2	2.3604(9)	2.4139(5)	2.3631(8)	2.7359(7)
222.4	2.3606(9)	2.4140(5)	2.3634(8)	2.7359(7)
231.6	2.3622(9)	2.4142(5)	2.3631(8)	2.7358(7)
240.6	2.3608(9)	2.4145(5)	2.3635(8)	2.7362(7)
249.8	2.3617(9)	2.4147(5)	2.3637(8)	2.7368(7)
259.1	2.3623(9)	2.4149(5)	2.3633(9)	2.7370(7)
268.3	2.3623(9)	2.4155(5)	2.3636(9)	2.7368(7)

when compared to the NaO_8 square antiprism, varying from 9.368 $Å^3$ at 2.5 K to 9.379 $Å^3$ at 265 K. The temperature dependence of the polyhedron volume is shown in Figure 13. In the same temperature interval, both the variance of the quadratic elongation, 1.0144 at 2.5 K, and the octahedron angle, 46.26 degrees squared at 2.5 K, increase approximately linearly with increasing temperature, the variation in the variance of the octahedron angle being a factor of ~6 greater than the equivalent variance for the NaO_8 square antiprism. The variations in quadratic elongation for both the AlO_6 and NaO_8 polyhedra were found to be approximately equal. The temperature dependence of the octahedron volume was fitted by an identical expression to that used for the NaO_8 polyhedron, with a derived characteristic frequency of 409 cm^{-1} and an estimated high-temperature volume-expansion coefficient of 1.9×10^{-5} K^{-1}.

Comparing the low-temperature Al–O distances with the high-temperature results of Cameron *et al.* (1973), written in parentheses, it was found that Al–O1A1 is the most strongly temperature-dependent, ranging from 1.987 Å at 2.5 K to 1.991 Å at 265 K (the highest increase with temperature), Al–O1A2 showed a weak decrease with temperature (the lowest increase with temperature), whereas Al–O2C1 was found to be invariant with temperature (intermediate increase with temperature). Within the octahedron, O1A1–Al–

TABLE 6. SELECTED BOND-ANGLES (°) AT THE SQUARE ANTIPRISMATIC SITE OF NaO_8 AS A FUNCTION OF TEMPERATURE (K)

Temp.	O1A1–Na–O3D1	O1A –Na–O3C1	O1A1–Na–O3D2	O2C2–Na–O2D2	O2C2–Na–O3D1	O2C2–Na–O3C2	O3C2–Na–O3D2
2.4	134.13(1)	121.68(1)	160.93(3)	153.52(4)	139.32(3)	114.62(1)	106.50(3)
10.3	134.13(1)	121.68(1)	160.98(3)	153.56(4)	139.28(3)	114.61(2)	106.46(3)
19.7	134.13(1)	121.69(1)	160.94(3)	153.52(4)	139.32(3)	114.62(2)	106.49(3)
29.5	134.13(1)	121.68(1)	160.95(3)	153.52(4)	139.32(3)	114.64(2)	106.48(3)
39.0	134.13(1)	121.68(1)	160.96(3)	153.54(4)	139.29(3)	114.63(2)	106.48(3)
47.5	134.12(1)	121.68(1)	160.95(3)	153.52(4)	139.32(3)	114.62(2)	106.48(3)
55.1	134.13(1)	121.67(1)	160.94(3)	153.53(4)	139.31(3)	114.62(2)	106.51(3)
64.0	134.13(1)	121.68(1)	160.94(3)	153.53(4)	139.31(3)	114.62(2)	106.50(3)
73.4	134.12(1)	121.69(1)	160.98(3)	153.57(4)	139.28(3)	114.62(2)	106.44(3)
83.0	134.13(1)	121.68(1)	160.96(3)	153.55(4)	139.29(3)	114.63(2)	106.47(3)
96.5	134.13(1)	121.69(1)	160.93(3)	153.52(4)	139.32(3)	114.63(2)	106.50(3)
106.4	134.12(1)	121.69(1)	160.96(3)	153.56(5)	139.29(3)	114.62(2)	106.46(3)
114.5	134.12(1)	121.70(1)	160.94(3)	153.53(5)	139.33(3)	114.62(2)	106.46(3)
121.9	134.12(1)	121.69(1)	160.94(3)	153.56(5)	139.29(3)	114.62(2)	106.49(3)
138.8	134.12(1)	121.70(1)	160.96(3)	153.56(4)	139.29(3)	114.64(2)	106.45(3)
149.6	134.13(1)	121.68(1)	160.98(3)	153.60(5)	139.26(3)	114.61(2)	106.43(3)
156.8	134.12(1)	121.68(1)	160.96(3)	153.57(5)	139.29(3)	114.62(2)	106.46(3)
165.9	134.12(1)	121.69(1)	160.99(3)	153.60(5)	139.28(3)	114.61(2)	106.40(3)
175.1	134.12(1)	121.69(1)	160.97(3)	153.61(5)	139.26(3)	114.62(2)	106.44(3)
184.5	134.13(1)	121.69(1)	160.98(3)	153.65(5)	139.23(3)	114.61(2)	106.43(3)
194.3	134.14(1)	121.68(1)	160.98(3)	153.65(5)	139.24(4)	114.60(2)	106.43(4)
203.6	134.11(1)	121.70(1)	160.96(3)	153.60(5)	139.28(4)	114.62(2)	106.44(4)
213.2	134.11(1)	121.70(1)	160.99(3)	153.64(5)	139.25(4)	114.61(2)	106.40(4)
222.4	134.12(1)	121.69(1)	160.97(3)	153.64(5)	139.26(4)	114.60(2)	106.41(4)
231.6	134.10(1)	121.70(1)	160.96(3)	153.64(5)	139.27(4)	114.59(2)	106.43(4)
240.6	134.11(1)	121.69(1)	160.99(3)	153.65(4)	139.25(4)	114.60(2)	106.41(4)
249.8	134.10(4)	121.68(1)	160.99(3)	153.68(5)	139.24(4)	114.59(2)	106.41(4)
259.1	134.10(1)	121.68(1)	160.98(3)	153.66(5)	139.25(4)	114.59(2)	106.42(4)
268.3	134.09(2)	121.69(1)	160.98(3)	153.65(5)	139.26(4)	114.58(2)	106.42(4)

O1A2, O1A1–Al–O1B2, O1A1–Al–O1B1 all decrease with increasing temperature, O1B2–Al–O2D1 and O2C1–Al–O2D1 are temperature-independent, and O1A1–Al–O2C1 and O1A2–Al–O2D1 both increase with increasing temperature. These low-temperature trends are broadly in keeping with the high-temperature results of Cameron *et al.* (1973). Bond-length and selected bond-angle variations are shown in Figure 14, and the bond lengths and angles are given in Tables 7 and 8, respectively. The position of the Al atom with respect to the center of the octahedron was found to be independent of temperature, with a displacement of 0.12 Å. The parameterization of the temperature dependence of the unit cell requires knowledge of the temperature variation of the lengths of the octahedron and tetrahedron edges. For jadeite at low temperatures, the edges O1A1–O1B2 and O1B2–O2D1 exhibit a decrease with increasing temperature, O1A1–O1A2 and O2C1–O2D1 are temperature-invariant, whereas O1A1–O1B1, O1A1–O2C1 and O1B2–O2C1 all increase with increasing temperature. The fractional change in edge distance with temperature is approximately constant for the edges that expand, and greater in magnitude than those that exhibit contraction. With the exception of O1B2–O2D1, which was found to be temperature-independent, the high-temperature results of Cameron *et al.* (1973) show all the octahedron edges to increase with increasing temperature.

The SiO_4 tetrahedron

The volume, angle variance and quadratic elongation of the SiO_4 tetrahedron were found to be constant between 2.5 and 265 K, with mean values of 2.179 $Å^3$, 22.2°[2] and 1.0054, respectively. The four bond-lengths in the tetrahedron show no significant variation with temperature, and neither do the three tetrahedron angles from oxygen O1A1. Of the remaining three tetrahedron angles, O2A2–Si–O3A1 and O2A2–Si–O3A2 show a slight decrease, and O3A1–Si–O3A2 shows a small increase with temperature. These conclusions agree broadly with the high-temperature results of Cameron *et al.* (1973), with the exception of the bond angles from O1A1, in which they found a decrease in bond angle to the atoms O3A1,2, and an increase in bond angle to O2A1. The temperature variation of the bond lengths and bond angles in the tetrahedra are shown in Tables 9 and 10, respectively.

In this low-temperature study, three of the six edge lengths in the tetrahedra are temperature-independent, O1A1–O3A1, O2A1–O3A1, O2A1–O3A2, and two show a weak increase with temperature, O1A1–O2A1, O1A1–O3A2. By contrast, the edge O3A1–O3A2, related to the length of the **c** axis, shows a strong increase with temperature, from 2.6137 Å at 2.5 K to 2.6148 Å at 265 K. The angle in the chain of tetrahedra, O3 – O3 – O3, increases approximately linearly from 174.2° to 174.4° over the same interval of temperature, indicating that only a small straightening of the chain occurs. Figure 15 shows the temperature variation of the edge distance O3A1–O3A2 and the associated chain angle between linked tetrahedra.

Cameron *et al.* (1973) found that the volume of the SiO_4 tetrahedron in aegirine, diopside, hedenbergite, jadeite, spodumene and ureyite increases only slightly with temperature over a wide range in temperature, whereas in this low-temperature study, the volume appears to remain constant. Defining the edge vector O3A2 → O1A1 as $\mathbf{r}_1$, O3A2 → O2A1 as $\mathbf{r}_2$, and O3A2

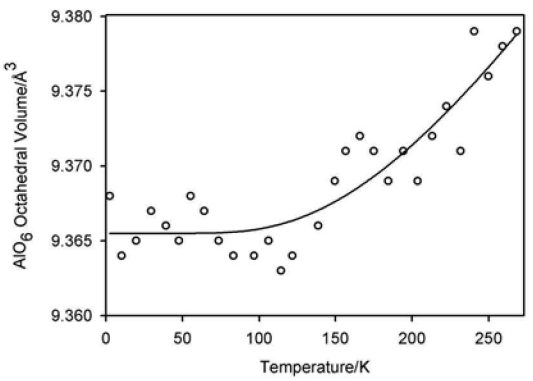

FIG. 13. The temperature dependence of the AlO_6 octahedron in jadeite. The full line shows a fit to these data assuming an Einstein model.

TABLE 7. BOND LENGTHS (Å) AT THE OCTAHEDRAL SITE OF AlO_6 AS A FUNCTION OF TEMPERATURE (K)

Temp.	Al – O1A1	Al – O1A2	Al – O2C1
2.4	1.9868(8)	1.9384(4)	1.8597(7)
10.3	1.9867(8)	1.9378(4)	1.8597(7)
19.7	1.9866(8)	1.9381(4)	1.8597(7)
29.5	1.9868(8)	1.9383(4)	1.8596(7)
39.0	1.9871(8)	1.9380(4)	1.8595(7)
47.5	1.9868(8)	1.9381(4)	1.8595(7)
55.1	1.9874(8)	1.9380(4)	1.8596(7)
64.0	1.9860(8)	1.9380(4)	1.8607(7)
73.4	1.9864(8)	1.9377(4)	1.8601(7)
83.0	1.9870(8)	1.9380(4)	1.8592(7)
96.5	1.9865(8)	1.9380(4)	1.8598(7)
106.4	1.9873(8)	1.9377(4)	1.8595(7)
114.5	1.9874(8)	1.9379(4)	1.8592(7)
121.9	1.9876(8)	1.9374(4)	1.8596(7)
138.8	1.9876(8)	1.9376(4)	1.8597(7)
149.6	1.9871(8)	1.9378(4)	1.8604(7)
156.8	1.9873(8)	1.9377(4)	1.8606(7)
165.9	1.9882(8)	1.9382(4)	1.8598(7)
175.1	1.9884(8)	1.9379(4)	1.8597(7)
184.5	1.9886(9)	1.9376(4)	1.8594(7)
194.3	1.9877(9)	1.9379(4)	1.8608(8)
203.6	1.9889(9)	1.9374(4)	1.8595(7)
213.2	1.9894(9)	1.9376(4)	1.8594(8)
222.4	1.9898(9)	1.9383(4)	1.8590(8)
231.6	1.9887(9)	1.9375(4)	1.8602(8)
240.6	1.9907(9)	1.9379(4)	1.8594(8)
249.8	1.9901(9)	1.9377(4)	1.8596(8)
259.1	1.9916(9)	1.9378(4)	1.8586(8)
268.3	1.9909(9)	1.9375(4)	1.8596(8)

TABLE 8. SELECTED BOND-ANGLES (°) AT THE OCTAHEDRAL SITE OF AlO_6 AS A FUNCTION OF TEMPERATURE (K)

Temp.	O1A1-Al-O1B1	O1A1-Al-O1B2	O1A1-Al-O1A2	O1A1-Al-O2C1	O1B2-Al-O2C1	O1B2-Al-O2D1	O2D1-Al-O2C1
2.4	86.51(4)	77.69(2)	96.00(3)	89.43(1)	89.86(2)	95.79(2)	97.32(5)
10.3	86.54(4)	77.68(2)	96.02(3)	89.43(2)	89.87(2)	95.78(2)	97.30(5)
19.7	86.51(4)	77.68(2)	96.01(3)	89.43(2)	89.87(2)	95.79(2)	97.33(5)
29.5	86.52(4)	77.70(2)	96.01(3)	89.44(2)	89.85(2)	95.79(2)	97.29(5)
39.0	86.52(4)	77.69(2)	96.01(3)	89.44(3)	89.86(2)	95.79(2)	97.31(5)
47.5	86.52(4)	77.69(2)	96.02(3)	89.44(2)	89.87(2)	95.78(2)	97.31(5)
55.1	86.49(4)	77.67(2)	96.00(3)	89.45(2)	89.87(2)	95.80(2)	97.32(5)
64.0	86.57(4)	77.71(2)	96.04(3)	89.44(2)	89.84(2)	95.77(2)	97.25(5)
73.4	86.57(4)	77.68(2)	96.03(3)	89.43(2)	89.85(2)	95.78(2)	97.27(5)
83.0	86.52(4)	77.66(2)	96.00(3)	89.44(2)	89.87(2)	95.81(2)	97.31(5)
96.5	86.53(4)	77.66(2)	96.02(3)	89.45(2)	89.86(2)	95.81(2)	97.29(5)
106.4	86.52(5)	77.64(3)	95.99(3)	89.44(2)	89.88(2)	95.83(2)	97.32(5)
114.5	86.48(4)	77.60(2)	95.97(3)	89.43(2)	89.90(2)	95.86(2)	97.38(5)
121.9	86.50(5)	77.62(3)	96.00(3)	89.45(2)	89.88(2)	95.85(2)	97.31(5)
138.8	86.52(4)	77.62(2)	95.99(3)	89.45(2)	89.84(2)	95.89(2)	97.31(5)
149.6	86.57(4)	77.65(2)	96.00(3)	89.44(2)	89.83(2)	95.86(2)	97.26(5)
156.8	86.54(4)	77.65(2)	96.01(2)	89.47(2)	89.83(2)	95.86(2)	97.25(5)
165.9	86.50(5)	77.63(3)	95.96(2)	89.44(2)	89.85(2)	95.89(2)	97.34(5)
175.1	86.52(4)	77.62(2)	95.96(3)	89.47(2)	89.84(2)	95.92(2)	97.28(5)
184.5	86.49(5)	77.59(2)	95.96(3)	89.48(2)	89.86(2)	95.93(2)	97.29(5)
194.3	86.59(5)	77.63(3)	95.97(3)	89.46(2)	89.82(2)	95.93(2)	97.23(5)
203.6	86.48(5)	77.54(3)	95.94(3)	89.48(2)	89.87(2)	95.97(2)	97.32(5)
213.2	86.48(5)	77.57(3)	95.94(2)	89.47(2)	89.85(2)	95.97(2)	97.33(5)
222.4	86.42(5)	77.55(3)	95.90(3)	89.48(2)	89.87(2)	95.98(2)	97.37(5)
231.6	86.52(5)	77.54(3)	95.94(3)	89.49(2)	89.86(2)	95.99(3)	97.26(5)
240.6	86.42(5)	77.56(3)	95.92(3)	89.49(2)	89.84(2)	96.00(3)	97.34(5)
249.8	86.46(5)	77.54(3)	95.91(3)	89.50(2)	89.85(2)	96.02(3)	97.29(5)
259.1	86.40(5)	77.50(3)	95.86(3)	89.49(2)	89.88(2)	96.06(3)	97.38(5)
268.3	86.43(5)	77.52(3)	95.91(3)	89.50(2)	89.84(3)	96.04(3)	97.34(6)

TABLE 9. BOND LENGTHS (Å) AT THE TETRAHEDRAL SITE OF SiO_4 AS A FUNCTION OF TEMPERATURE (K)

Temp.	Si – O1A1	Si – O2A1	Si – O3A1	Si – O3A2
2.4	1.6387(6)	1.5897(6)	1.6259(6)	1.6395(6)
10.3	1.6383(6)	1.5905(6)	1.6258(6)	1.6394(6)
19.7	1.6391(6)	1.5896(6)	1.6263(6)	1.6393(6)
29.5	1.6386(6)	1.5897(6)	1.6264(6)	1.6392(6)
39.0	1.6390(6)	1.5897(6)	1.6255(6)	1.6398(6)
47.5	1.6389(6)	1.5896(6)	1.6263(6)	1.6392(6)
55.1	1.6393(6)	1.5890(6)	1.6254(6)	1.6396(6)
64.0	1.6389(6)	1.5893(6)	1.6257(6)	1.6397(6)
73.4	1.6391(6)	1.5900(6)	1.6258(6)	1.6392(6)
83.0	1.6390(6)	1.5899(6)	1.6257(6)	1.6394(6)
96.5	1.6390(6)	1.5896(6)	1.6259(6)	1.6397(6)
106.4	1.6391(6)	1.5899(6)	1.6261(6)	1.6390(6)
114.5	1.6398(6)	1.5896(6)	1.6261(6)	1.6390(6)
121.9	1.6386(6)	1.5899(6)	1.6256(6)	1.6401(6)
138.8	1.6390(6)	1.5898(6)	1.6262(6)	1.6397(6)
149.6	1.6387(6)	1.5895(6)	1.6264(6)	1.6398(6)
156.8	1.6388(6)	1.5893(6)	1.6265(6)	1.6398(6)
165.9	1.6390(6)	1.5894(6)	1.6265(6)	1.6402(6)
175.1	1.6385(6)	1.5895(6)	1.6261(6)	1.6403(6)
184.5	1.6395(6)	1.5898(6)	1.6254(6)	1.6402(6)
194.3	1.6389(6)	1.5898(6)	1.6252(6)	1.6400(6)
203.6	1.6394(6)	1.5897(6)	1.6263(6)	1.6400(6)
213.2	1.6397(6)	1.5902(6)	1.6259(6)	1.6401(6)
222.4	1.6392(6)	1.5904(6)	1.6260(6)	1.6401(6)
231.6	1.6400(6)	1.5898(6)	1.6260(6)	1.6396(6)
240.6	1.6386(6)	1.5907(6)	1.6264(6)	1.6400(6)
249.8	1.6391(6)	1.5902(6)	1.6262(6)	1.6399(6)
259.1	1.6393(6)	1.5905(6)	1.6254(6)	1.6404(6)
268.3	1.6396(6)	1.5905(6)	1.6257(6)	1.6402(6)

→ O3A1 as $\mathbf{r}_3$, the following expression is required to hold for all temperatures if the volume is to be invariant with change in temperature:

$$\mathbf{r}_1 \times \mathbf{r}_2 \cdot \frac{d\mathbf{r}_3}{dT} + \mathbf{r}_1 \times \frac{d\mathbf{r}_2}{dT} \cdot \mathbf{r}_3 + \frac{d\mathbf{r}_1}{dT} \times \mathbf{r}_2 \cdot \mathbf{r}_3 = 0 = \left(\frac{6dV_{tet}}{dT} \right)$$

As the edge lengths of the tetrahedra only begin to move away from saturated behavior at ~100 K, this temperature has been chosen as the reference from which the derivatives have been calculated as $d\mathbf{r}_i/dT \approx [\mathbf{r}_i(T) - \mathbf{r}_i(100)]/(T - 100)$. The results from the expression were checked for consistency by calculating $[V_{tet}(T) - V_{tet}(100)]/(T - 100)$, where V_{tet} is the volume of the SiO_4 tetrahedron. Despite the fact that these calculations are at the limit of the precision that could be derived from the data, the following two observations were found for all but one of the 18 temperatures above the reference temperature

$$\mathbf{r}_1 \times \mathbf{r}_2 \cdot \frac{d\mathbf{r}_3}{dT} > \frac{d\mathbf{r}_1}{dT} \times \mathbf{r}_2 \cdot \mathbf{r}_3 > 0$$

$$\mathbf{r}_1 \times \frac{d\mathbf{r}_2}{dT} \cdot \mathbf{r}_3 < 0$$

The tentative conclusions from these observations is that the constant volume of the SiO_4 tetrahedron in jadeite at low temperatures is maintained by a close balancing of the action of O2A1, which moves toward the tetrahedron face containing $\mathbf{r}_1$ and $\mathbf{r}_3$, with that of O3A1, which moves away from the face containing $\mathbf{r}_1$ and $\mathbf{r}_2$. The latter is identified as arising from the opening of the tetrahedron edge that governs the thermal expansion of the **c** axis, which is discussed in more detail in a following section.

Inter-polyhedron torsion angles

The torsion angle, τ, between neighboring polyhedra can be defined by the expression

$$\cos(\tau) = \frac{(\mathbf{n}_1 \cdot \mathbf{n}_2)}{n_1 n_2}$$

$$\mathbf{n}_1 = \mathbf{r}_1 \times \mathbf{r}_2$$

$$\mathbf{n}_2 = \mathbf{r}_3 \times \mathbf{r}_4$$

where $\mathbf{r}_1$ and $\mathbf{r}_2$ are vectors from one central cation to two polyhedron ligands, one of which is shared by the second central cation. Vectors $\mathbf{r}_3$ and $\mathbf{r}_4$ are from the second central cation to the shared ligand and an additional ligand within its coordination polyhedron. In the case of the neighboring edge-sharing AlO_6 octahedra in jadeite, both ligands are shared; with the vectors defined as $\mathbf{r}_1$ from *M*1H to O1D2, $\mathbf{r}_2$ from *M*1H to O1C1, $\mathbf{r}_3$ from *M*11H to O1C1 and $\mathbf{r}_4$ from *M*11H to O1D2, τ is 0° and independent of unit-cell parameters. For the AlO_6 ribbon, τ has no pressure or temperature dependence because $\mathbf{r}_1$ and $\mathbf{r}_2$ always remain antiparallel to $\mathbf{r}_3$ and $\mathbf{r}_4$, respectively.

The torsion angle between the bases of adjacent SiO_4 tetrahedra along the chain of tetrahedra (Fig. 16) is constant at ~3.21° throughout the whole interval of temperature. This torsion angle is related to the tilting of the normal to one of the bases with respect to **a***, angle

TABLE 10. BOND ANGLES (°) AT THE TETRAHEDRAL SITE OF SiO_4 AS A FUNCTION OF TEMPERATURE (K)

Temp.	O1A1-Si-O2A1	O1A1-Si-O3A1	O1A1-Si-O3A2	O2A1-Si-O3A1	O2A1-Si-O3A2	O3A1-Si-O3A2
2.4	118.39(3)	107.62(3)	107.21(3)	110.52(3)	106.08(3)	106.34(3)
10.3	118.41(3)	107.61(3)	107.25(3)	110.50(3)	106.05(3)	106.35(3)
19.7	118.45(3)	107.60(3)	107.22(3)	110.51(3)	106.10(3)	106.33(3)
29.5	118.41(3)	107.61(3)	107.24(3)	110.50(3)	106.08(3)	106.33(3)
39.0	118.39(3)	107.61(3)	107.22(3)	110.54(3)	106.07(3)	106.34(3)
47.5	118.42(3)	107.58(3)	107.21(3)	110.53(3)	106.09(3)	106.34(3)
55.1	118.40(3)	107.58(3)	107.19(3)	110.56(3)	106.09(3)	106.36(3)
64.0	118.41(4)	107.60(3)	107.20(3)	110.54(3)	106.08(3)	106.34(3)
73.4	118.39(4)	107.60(3)	107.24(3)	110.52(3)	106.07(3)	106.36(3)
83.0	118.41(4)	107.61(3)	107.21(3)	110.52(3)	106.07(3)	106.36(3)
96.5	118.42(3)	107.61(3)	107.21(3)	110.51(3)	106.08(3)	106.33(3)
106.4	118.40(4)	107.60(3)	107.25(3)	110.50(3)	106.07(3)	106.36(3)
114.5	118.40(4)	107.60(3)	107.21(3)	110.55(3)	106.06(3)	106.35(3)
121.9	118.44(4)	107.63(3)	107.24(3)	110.49(3)	106.03(3)	106.33(3)
138.8	118.41(3)	107.62(3)	107.26(3)	110.48(3)	106.07(3)	106.33(3)
149.6	118.44(4)	107.59(3)	107.23(3)	110.56(3)	106.08(3)	106.32(3)
156.8	118.45(4)	107.60(3)	107.23(3)	110.50(3)	106.07(3)	106.31(3)
165.9	118.43(3)	107.63(3)	107.20(3)	110.55(3)	106.05(3)	106.30(3)
175.1	118.46(4)	107.63(3)	107.23(3)	110.48(3)	106.05(3)	106.32(3)
184.5	118.44(4)	107.61(3)	107.21(3)	110.50(3)	106.06(3)	106.36(3)
194.3	118.42(4)	107.61(3)	107.20(3)	110.50(3)	106.06(4)	106.38(3)
203.6	118.46(4)	107.62(3)	107.25(3)	110.48(3)	106.03(3)	106.33(3)
213.2	118.41(4)	107.63(3)	107.24(3)	110.50(3)	106.05(4)	106.35(3)
222.4	118.43(4)	107.65(3)	107.22(3)	110.48(3)	106.04(4)	106.35(3)
231.6	118.46(4)	107.59(3)	107.20(3)	110.50(4)	106.05(4)	106.38(3)
240.6	118.42(4)	107.66(3)	107.28(3)	110.44(4)	106.03(4)	106.35(3)
249.8	118.46(4)	107.62(3)	107.23(3)	110.46(4)	106.03(4)	106.36(3)
259.1	118.44(4)	107.64(3)	107.21(3)	110.51(4)	106.00(4)	106.38(3)
268.3	118.42(4)	107.63(4)	107.22(3)	110.49(4)	106.03(4)	106.38(3)

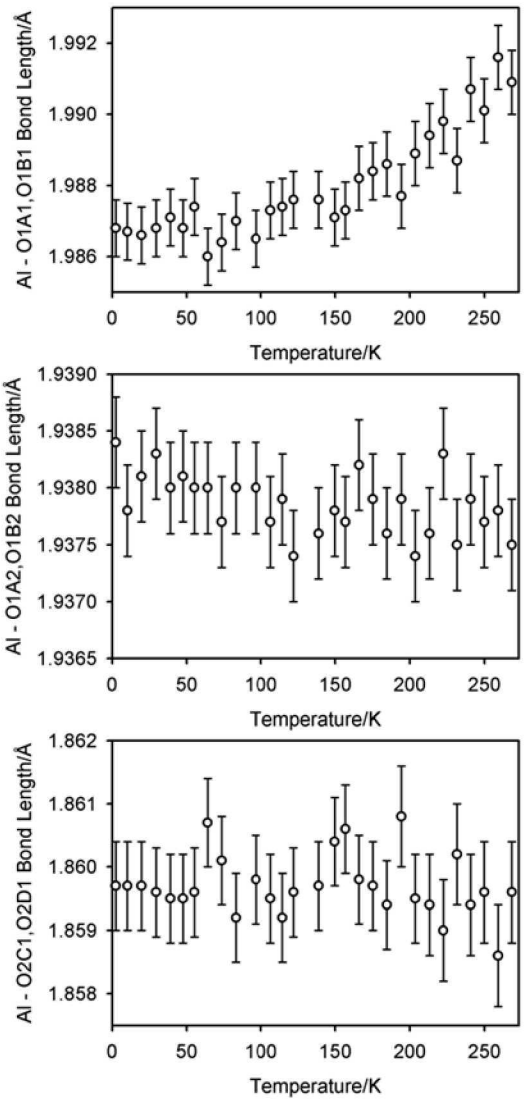

FIG. 14. The temperature dependence of the three independent Al–O bond lengths and of four of the O–Al–O bond angles in jadeite.

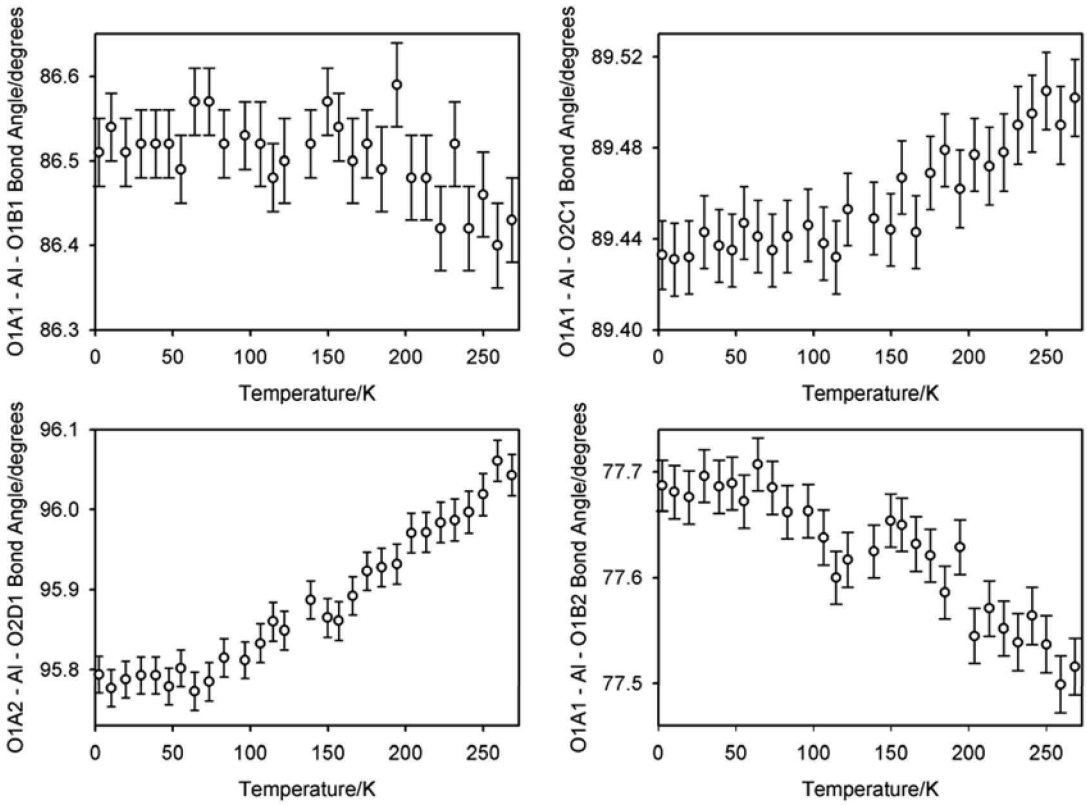

ζ, and the angle the projection of this normal to the $b-c$ plane makes with **c**, angle ξ, through the expression

$$\tau \approx 2\zeta\sqrt{1-(\xi-\pi/2)^2}$$

As ζ is small, 1.61° at 265 K, and ξ is slightly greater than 90°, 92.80° at 265 K, τ can be shown to be approximately 2ζ. The angles ζ and ξ can be identified with the tilt and azimuthal tilt angles, respectively, in the structural study of the jadeite – diopside solid-solution series by Boffa Ballaran *et al.* (1997).

The torsion angles between the AlO_6 octahedron and the SiO_4 tetrahedron do, however, show temperature variations. Figure 17 illustrates the two independent torsion angles for a path through the jadeite structure separated by the lattice vector **b**. Angle $\tau 1$ is derived from the vectors *M*1 to O1B1 ($\mathbf{r_1}$), *M*1 to O2D1 ($\mathbf{r_2}$), *T*1B to O1B1 ($\mathbf{r_3}$) and *T*1B to O2B1 ($\mathbf{r_4}$). Angle $\tau 2$ is derived from the vectors *T*1B to O1B1 ($\mathbf{r_1}$), *T*1B to O2B1 ($\mathbf{r_2}$), *M*11 to O2B1 ($\mathbf{r_3}$) and *M*11 to O1D1 ($\mathbf{r_4}$). Neither $\tau 1$ nor $\tau 2$ show a strong temperature-dependence, but both exhibit a trend to decrease with increasing temperature (Fig. 18). Similar calculations can be performed for the two torsion angles described by a path separated by the lattice vector **a** (Fig. 19). In this case, $\tau 1$ is derived from the vectors *M*1 to O1B1 ($\mathbf{r_1}$), *M*1 to O1A1 ($\mathbf{r_2}$), *T*1A to O1A1 ($\mathbf{r_3}$) and *T*1A to O2A1 ($\mathbf{r_4}$), and $\tau 2$ is derived from the vectors *T*1A to O1A1 ($\mathbf{r_1}$), *T*1A to O2A1 ($\mathbf{r_2}$), *M*1H to O2B1 ($\mathbf{r_3}$) and *M*1H to O2A1 ($\mathbf{r_4}$). Angle $\tau 1$ shows a weak tendency to increase with increasing temperature, whereas $\tau 2$ shows a marked decrease with increasing temperature. Unfortunately, the changes in these four torsion angles are too small to unambiguously identify the structural basis for the observed temperature-dependence.

Bond-valence sums

Bond-valence sums for jadeite at 268 K, calculated using the parameters from Brown & Altermatt (1985), show the Na cation to be highly overbonded (1.42 valence units, *vu*), Al to be underbonded (2.87 *vu*) and the Si to be charge-balanced (4.00 *vu*). For the anions, results typical of a clinopyroxene were found (Cameron & Papike 1980); O1 is close to charge-balanced (2.04 *vu*), O2 is underbonded (1.86 *vu*) and O3 is overbonded (2.25 *vu*), these values being in excellent agreement

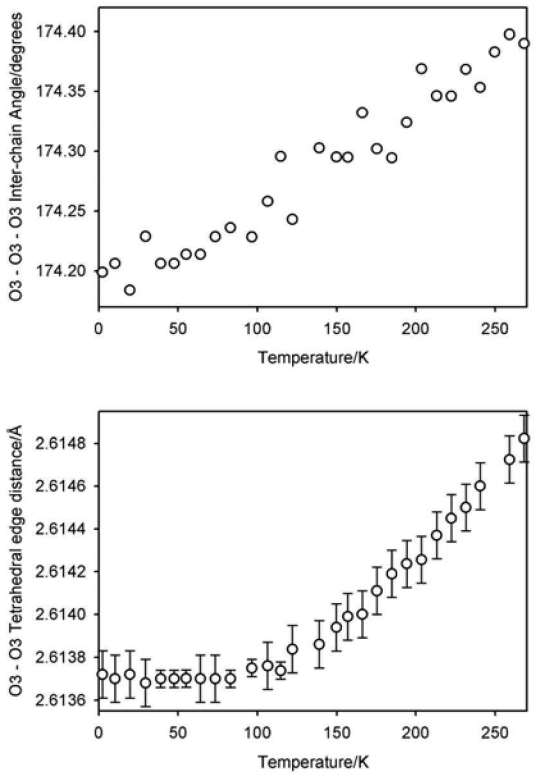

FIG. 15. The temperature variation of the O3–O3–O3 inter-chain angle and the O3–O3 tetrahedron-edge distance in jadeite. The temperature dependence of the thermal expansion coefficient of the lattice parameter *c* is related to these two variations, with 99% of the thermal expansion taken up by the extension of the tetrahedron edge.

with the results of Cameron *et al.* (1973) for an ambient temperature. The temperature dependence of the bond-valence sum for all atoms is minimal; all exhibit a small, monotonic decrease with increasing temperature owing to the lengthening of cation–oxygen bond distances.

PARAMETERIZATION OF THE TEMPERATURE DEPENDENCE OF THE UNIT-CELL EDGES

To derive a rigorous structural basis for the thermal expansion behavior of clinopyroxenes is problematic, the difficulty arising primarily from the non-orthogonality of the unit-cell basis vectors. With the exception of the **c** axis, it does not appear possible to find two atomic positions within the clinopyroxene structure that not only are separated by a single lattice vector but also exhibit a connected path of polyhedra that only spans a two-dimensional, orthogonal subspace. To a good approximation, the temperature dependence of β can be ignored, and in this section, we derive a basis for the thermal expansion of the three unit-cell axes. As noted earlier, the temperature variation of β mimics that of the thermal expansion tensor, the orientation of which is related to the bonding of the Na–O square antiprism.

The c axis

Figure 16 shows the structure of jadeite viewed down **a***, with the atoms O3C1 and O3C1' separated by **c**, and with the vectors from O3C2, $\mathbf{r}_1$ and $\mathbf{r}_2$, lying in the plane spanned by **b** and **c**. Hence

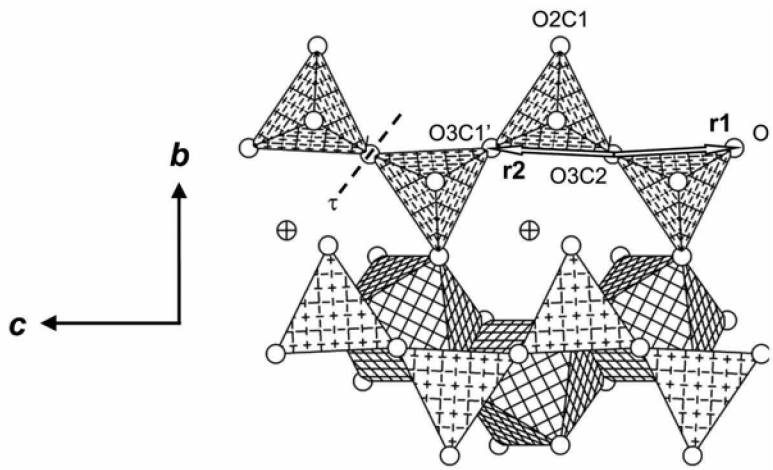

FIG. 16. A connected polyhedron part of the crystal structure of jadeite viewed down **a***. Thermal expansion of the *c* axis is related to the orientation and magnitude of the tetrahedron-edge vectors **r1** and **r2**. The torsion angle τ is described in the text.

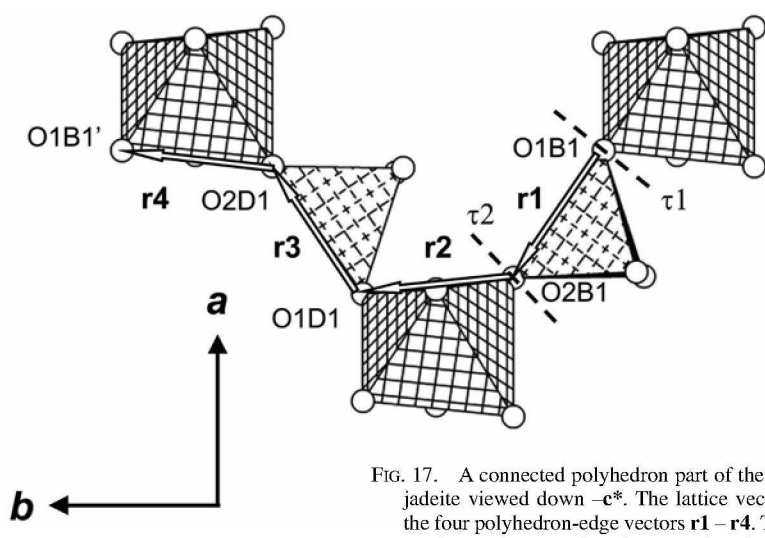

FIG. 17. A connected polyhedron part of the crystal structure of jadeite viewed down $-\mathbf{c}^*$. The lattice vector **b** is the sum of the four polyhedron-edge vectors **r1** – **r4**. The two polyhedron torsion angles $\tau 1$ and $\tau 2$ between the edges of octahedra and tetrahedra are illustrated.

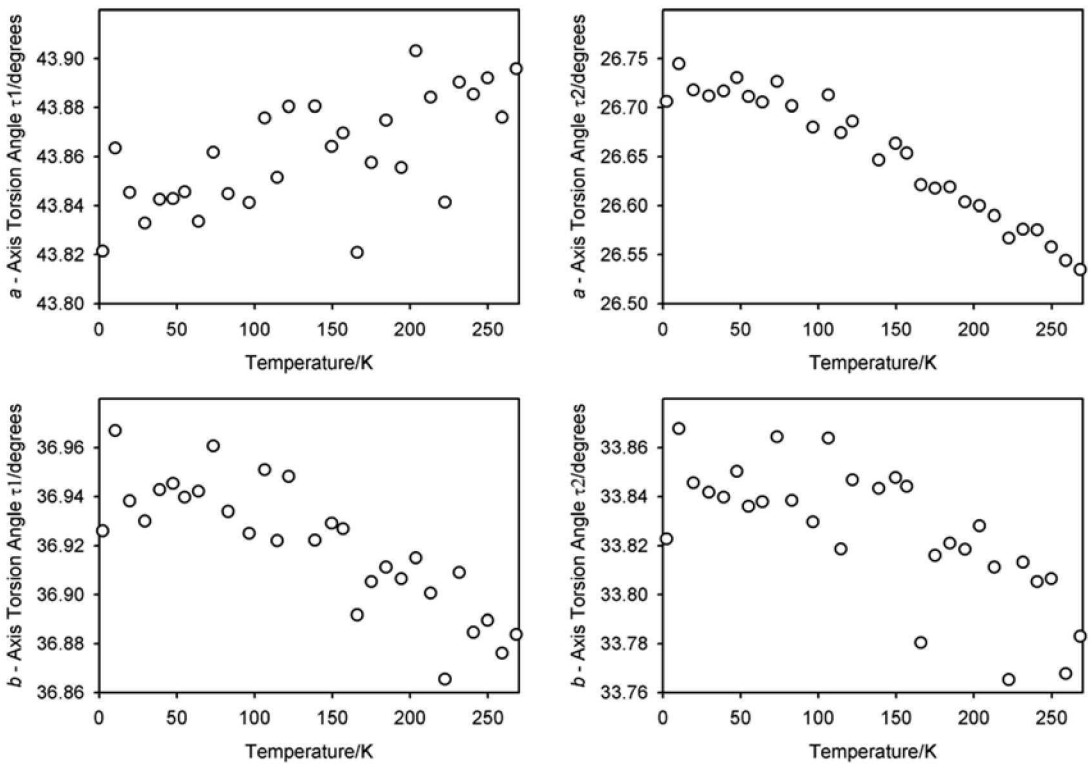

FIG. 18. The temperature dependence of the torsion angles $\tau 1$ and $\tau 2$ for the *a* and *b* axes of jadeite, described in the text, and shown diagramatically in Figures 17 and 19.

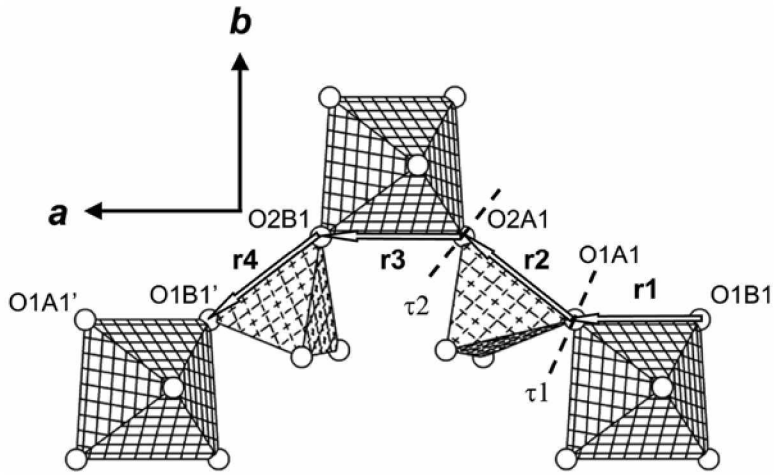

FIG. 19. A connected polyhedron part of the crystal structure of jadeite viewed down $-\mathbf{c}^*$. The lattice vector **a** is the sum of the four polyhedron-edge vectors **r1** – **r4**. The two polyhedron torsion angles $\tau 1$ and $\tau 2$ between the edges of octahedra and tetrahedra are illustrated.

$$c = 2r_1 \sin\left(\frac{\phi}{2}\right)$$

$$\frac{1}{c}\frac{dc}{dT} = \frac{1}{r_1}\frac{dr_1}{dT} + \frac{1}{2}\cot\left(\frac{\phi}{2}\right)\frac{d\phi}{dT}$$

where ϕ is the chain angle among the tetrahedra and r1 is the length of the O3 – O3 tetrahedron edge. For temperatures greater than ~100 K, $dr_1/r_1dT >> 0.5\cot(\phi/2)d\phi/dt$; to a very good approximation, the expansion of the c axis is purely governed by the rate of change of the length of the O3 – O3 tetrahedron edge and not by the straightening of the chain of tetrahedra. Using the Einstein parameterization for the temperature dependence of the c axis, dc/cdT (280 K) = $3.67 \times 10^{-6}\,K^{-1}$, and $dr_1/r_1dT = 3.64 \times 10^{-6}\,K^{-1}$, *i.e.*, 99% of the expansion is taken up by the expansion of the tetrahedron edge.

The b axis

Figure 17 shows a path through the clinopyroxene structure from O1B1 in one unit cell to the identical atom in the neighboring unit-cell (O1B1'), separated by the lattice vector **b**.

$$\mathbf{b} = \sum_{i=1}^{4} \mathbf{r}_i$$

The path length is characterized by the tetrahedron edge-length from O1B1 to O2B1, r_1 and its associated direction cosine with respect to **b**, n_1, and the octahedron edge-length from O2B1 to O1D1, r_2 and its associated direction cosine with respect to **b**, n_2.

$$b = 2r_1 \times n_1 + 2r_2 \times n_2$$

The expression above illustrates the difficulty of parameterizing the cell dimensions in terms of simple derived structural quantities such as bond lengths and bond angles; it is necessary to know the explicit temperature-dependence of the direction cosine components of the edge vectors *a priori*. Despite this apparent difficulty, the direction cosine components would not be expected to show a large variation with temperature in the clinopyroxene structure owing to the rigidity of the edge-shared octahedra. However, neither can it be safely assumed that they are constant in temperature. A Taylor's expansion would suggest that a linear dependence on temperature is to be expected. Figure 18 shows that this is indeed the case for the required components to parameterize the temperature variation of the **b** axis. For temperatures greater than 100 K, both the octahedron and tetrahedron edge-lengths are found to be approximately linear with increasing temperature. Differentiating the expression and substituting for the temperature dependencies of the edge lengths and direction cosines shows that the opening of the octahedron edges are the dominant structural mechanism for the expansion of the *b* axis at low temperatures (~73%). The opening of the tetrahedron edge-lengths are a factor of about four times smaller, and the changes due

to orientational effects are even smaller still. At room temperature, the fractional change in the *b* axis with temperature using the Einstein parameterization is 7.4 $\times$ 10^{-6} K^{-1} and 7.1 $\times$ 10^{-6} K^{-1} using the polyhedron-edge parameterization discussed above.

The a axis

Figure 19 shows a path through the clinopyroxene structure from O1A1 in one unit cell to the identical atom in the neighboring unit-cell (O1A1') separated by the lattice vector **a**.

$$\mathbf{a} = \sum_{i=1}^{4} \mathbf{r}_i$$

The path length is characterized by two octahedron edge-lengths, the first from O1B1 to O1A1, r_1 and its associated direction cosine with respect to **a**, n_1, the second, from O2A1 to O2B1, r_3 with its associated direction cosine, n_3, and the tetrahedron edge-length from O1A1 to O2A1, r_2 and corresponding direction cosine, n_2.

$$a = r_1 \times n_1 + 2r_2 \times n_2 + r_3 \times n_3$$

Using the same method of data analysis as carried out for the b axis was not as successful in this case, with the calculated coefficient of thermal expansion being 4.2 $\times$ 10^{-6} K^{-1} at room temperature, in comparison with an observed value of 5.2 $\times$ 10^{-6} K^{-1} using the Einstein parameterization. However, empirically refitting the data using expressions that were saturated at low temperature, becoming linear at high temperature was much more successful with a calculated coefficient of thermal expansion of 5.4 $\times$ 10^{-6} K^{-1}. The structural basis for the thermal expansion of this axis is more complex than for the *b* axis, reflecting the larger number of independent, interacting polyhedra. Although both octahedron edges run almost parallel to **a** and naively might be predicted to dominate this effect, the opposite is in fact found. The octahedron edge O2A1–O2B1 shows negligible thermal expansion, and, although the opening of the octahedron edge O1A1–O1B1 comprises 38% of the calculated thermal expansion, its change in orientation contributes a 14% contraction. Somewhat surprisingly, it is the change in both the tetrahedron edge-length and its orientation that contribute 63% to the overall expansion. The relative difficulty in determining a reliable parameterization to accurately predict the fractional expansion of the *a* axis probably lies with the small magnitude of the changes in both the octahedron edge-length O2A1–O2B1 and the tetrahedron edge-length O1A1–O2A1. It would be of interest to attempt this analysis with data collected at much higher temperatures, or, indeed pressure, where the changes in the polyhedra will be significantly larger and will thus enable a more precise structural basis for this axis to be derived.

Conclusions

For many years, the polyhedron approach to crystal chemistry pioneered by Hazen & Finger (1982) and Finger & Hazen (2000) has been of great benefit to mineral physicists, allowing predictions to be made of crystal structure in terms of both temperature and pressure. The advent of third-generation synchrotrons, state-of-the-art accelerator sources of neutrons, and large area-detectors on laboratory-based X-ray single-crystal diffractometers now offers opportunities to re-examine the temperature and pressure dependence of the crystal structures of major rock-forming minerals with a new level of detail. In this paper, we show that using a high-flux neutron source, coupled with a high count-rate, and a high-resolution powder diffractometer, it is possible to derive:

1) the temperature dependence of the unit cell with a precision of a few parts in 10^5, in data-collection times of the order of twenty-five minutes, with temperature stabilities of less than 0.5 K. This allows the subtleties in the temperature variation of thermal expansion tensor to be investigated and related to changes in the crystal (or magnetic) structures of the pyroxene under investigation.

2) the temperature variation of the unit-cell volume at a precision that allows the temperature dependence of the thermodynamic Grüneisen parameter of a pyroxene to be determined for the first time. Using simple statistical mechanical models, the Debye and Einstein temperatures may also be derived from these data and compared to values obtained directly through calorimetry, or indirectly, through vibrational spectroscopy.

3) highly precise crystal structures from data collections of the order of 1 hour with a Q maximum resolution of 20 $Å^{-1}$. The ability to collect data rapidly, under controlled thermodynamic conditions, allows the subtle changes in the crystal structure or atomic vibrations to be determined directly without having to resort to parametric methods of data analysis. These data have provided a model of the structural basis for the thermal expansion of a jadeite along the three crystallographic unit-cell edges. Owing to the magnitude of the Q-space resolution,the precise determination of the atomic displacement parameters has allowed the derivation of the vibrational Debye temperatures of a pyroxene for the first time.

Acknowledgements

This paper is dedicated to the memory of Joseph V. Smith, who made major contributions to our understanding of many minerals and geochemical processes,

both terrestrial and lunar. In this publication, we have attempted to understand the behavior of jadeite using an analysis that owes much to the crystallographic insight that Joe Smith brought to the feldspars and the polymorphs of $MgSiO_3$. GDP personally benefitted from, and enjoyed, working with Professor Smith during a year in Chicago in the 1980s.

The authors are particularly grateful to Professor Robert F. Martin for handling this manuscript, and for the enlightened policy of *The Canadian Mineralogist* in allowing such a lengthy manuscript to be published *in toto*. Careful and critical refereeing was carried out by Professor M.T. Dove and Dr. M. Tribaudino, to whom we are indebted for improving the manuscript significantly. Thanks are due to Dr. P.F. Schofield (Natural History Museum) for providing the material used in this study, to Professor C.M.B. Henderson (University of Manchester) for facilitating the electron-microprobe analyses, and Mr. D.A. Plant (University of Manchester) for carrying out this analysis. KSK is particularly grateful to Dr. I.G. Wood (University College, London) for the many useful discussions that have helped this work to progress.

References

Ballet, O., Coey, J.M.D., Fillion, G., Ghose, A., Hewat, A.W. & Regnard, J.R. (1989): Magnetic order in acmite, $NaFeSi_2O_6$. *Phys. Chem. Minerals* **16**, 672-677.

Barron, T.H.K. & White, G.K. (1999): *Heat Capacity and Thermal Expansion at Low Temperatures*. Kluwer Academic, New York, N.Y.

Boffa Ballaran, T., Carpenter, M.A., Domeneghetti, M.C. & Tazzoli, V. (1997): Hard mode infrared spectroscopy of cation ordering and substitution in a chain silicate. *Phase Transitions* **63**, 159-170.

Bowey, J.E., Lee, C., Tucker, C., Hofmeister, A.M., Ade, P.A.R. & Barlow, M.J. (2001): Temperature effects on the 15–85 μm spectra of olivines and pyroxenes. *Monthly Notices, R. Astron. Soc.* **325**, 886-896.

Brown, I.D. & Altermatt, D. (1985): Bond-valence parameters obtained from a systematic analysis of the inorganic crystal structure database. *Acta Crystallogr.* **B41**, 244-247.

Brown, P.J. & Matthewman, J.C. (1993): The Cambridge crystallography subroutine library. *Rutherford Appleton Lab., Rep.* **RAL-93-009**.

Burnham, C.W., Clark, J.R., Papike, J.J. & Prewitt, C.T. (1967): A proposed crystallographic nomenclature for clinopyroxene structures. *Z. Kristallogr.* **125**, 109-119.

Cameron, M. & Papike, J.J. (1980): Crystal chemistry of silicate pyroxenes. *In* Pyroxenes (C.T. Prewitt, ed.). *Rev. Mineral.* **7**, 5-92.

Cameron, M., Sueno, S., Prewitt, C.T. & Papike, J.J. (1973): High-temperature crystal chemistry of acmite, diopside, hedenbergite, jadeite, spodumene and ureyite. *Am. Mineral.* **58**, 594-618.

David, W.I.F., Ibberson, R.M. & Matthewman, J.C. (1992): Profile analysis of neutron powder diffraction data at ISIS. *Rutherford Appleton Lab., Rep.* **RAL-92-032**.

Dietrich, P. & Arndt, J. (1982): Effects of pressure and temperature on the physical behavior of mantle-relevant olivine, orthopyroxene and garnet. I. Compressibility, thermal properties and macroscopic Grüneisen parameters. *In* High-Pressure Researches in Geosciences (W. Schreyer, ed.). E. Schweizerbart'sche Verlagsbuchhandlung, Stuttgart, Germany (293-306).

Finger, L.W. & Hazen, R.M. (2000): Systematics of high-pressure silicate structures. *In* High-Temperature and High-Pressure Crystal Chemistry (R.M. Hazen & R.T. Downs, eds.). *Rev. Mineral.* **41**, 123-155.

Finger, L.W. & Ohashi, Y. (1976): The thermal expansion of diopside to 800°C and a refinement of the crystal structure at 700°C. *Am. Mineral.* **61**, 303-310.

Fortes, A.D., Wood, I.G., Alfredsson, M., Vočadlo, L. & Knight, K.S. (2005): The incompressibility and thermal expansivity of D_2O ice II determined by powder neutron diffraction. *J. Appl. Crystallogr.* **38**, 612-618.

Ghose, S., Hewat, A.W., Van Dang, N. & Weidner, J.R. (1988): Magnetic phase transitions in quasi-one dimensional antiferromagnets: ferrosilite, $Fe_2Si_2O_6$, and hedenbergite, $CaFeSi_2O_6$. *Mater. Sci. Forum* **27/28**, 235-242.

Hattori, T., Nagai, T., Yamanaka, T., Werner, S. & Schulz, H. (2000): Single-crystal X-ray diffraction study of $FeGeO_3$ high-P clinopyroxene (*C2/c*) up to 8.2 GPa. *Am. Mineral.* **85**, 1485-1491.

Hazen, R.M. & Finger, L.W. (1982): *Comparative Crystal Chemistry*. John Wiley and Sons, New York, N.Y.

Hemingway, B.S., Bohlen, S.R., Hankins, W.B., Westrum, E.F., Jr. & Kuskov, O.L. (1998): Heat capacity and thermodynamic properties for coesite and jadeite, reexamination of the quartz–coesite equilibrium boundary. *Am. Mineral.* **83**, 409-418.

Herpin, P., Whuler, A., Boucher, B. & Sougi, M. (1971): Étude cristallographique et magnétique de $MnGeO_3$. *Physica status solidi (b)* **44**, 71-84.

James, R.W. (1962): *The Optical Principles of the Diffraction of X-Rays*. G. Bell and Sons Ltd., London, U.K.

Kandelin, J. & Weidner, D.J. (1988): The single-crystal elastic properties of jadeite. *Phys. Earth Planet. Int.* **50**, 251-260.

Kieffer, S.W. (1979): Thermodynamics and lattice vibrations of minerals. 1. Mineral heat capacities and their relation-

ships to simple lattice vibrational models. *Rev. Geophys. Space Phys.* **17**, 1-19.

KNIGHT, K.S. (1996): A neutron powder diffraction determination of the thermal expansion tensor of crocoite ($PbCrO_4$) between 60 K and 290 K. *Mineral. Mag.* **60**, 963-972.

KNIGHT, K.S. (2001a): The temperature dependence of the nuclear and magnetic structure of hedenbergite, ISIS Facility Annual Report 2000–2001. *Rutherford Appleton Lab., Rep.* **RAL-TR-2001-50, RB12199**.

KNIGHT, K.S. (2001b): Determination of the magnetostriction tensor in hedenbergite, ISIS Facility Annual Report 2000–2001. *Rutherford Appleton Lab., Rep.* **RAL-TR-2001-50, RB12200**.

KNIGHT, K.S., STETTON, I.C. & SCHOFIELD, P.F. (1999): Temperature evolution between 50 K and 320 K of the thermal expansion tensor of gypsum derived from neutron powder diffraction data. *Phys. Chem. Minerals* **26**, 477-483.

KNIGHT, K.S., ZOCHOWSKI, S.W. & SCHOFIELD, P.F. (2000): Low temperature structural studies of Na clinopyroxenes. *ISIS Facility Annual Report 1999–2000. Rutherford Appleton Lab., Rep.* **RAL-TR-2000-50, RB10764**.

LARSON, A.C. & VON DREELE, R.B. (1988): GSAS general structure analysis system. *Los Alamos Nat. Lab.*, **LAUR 86-748**.

LOTTERMOSER, W., REDHAMMER, G., FORCHER, K., AMTHAUER, G., PAULUS, W., ANDRÉ, G. & TREUTMANN, W. (1998): Single crystal Mössbauer and neutron powder diffraction measurements on the synthetic clinopyroxene Li-acmite $LiFeSi_2O_6$. *Z. Kristallogr.* **213**, 101-107.

LUMSDEN, M.D., GRANROTH, G.E., MANDRUS, D., NAGLER, S.E., THOMPSON, J.R., CASTELLAN, J.P. & GAULIN, B.D. (2000): Long-range antiferromagnetic order in the S=1 chain compound $LiVGe_2O_6$. *Phys. Rev. B* **62**, R9244-R9247.

MCCARTHY, A.C., DOWNS, R.T. & THOMPSON, R.M. (2008): Compressibility trends of the clinopyroxenes, and an in-situ high-pressure single-crystal X-ray diffraction study of jadeite. *Am. Mineral.* **93**, 198-209.

MOLSTER, F.J., WATERS, L.B.F.M. & TIELENS, A.G.G.M. (2002b): Crystalline silicate dust around evolved stars. II. The crystalline silicate complexes. *Astronomy and Astrophysics* **382**, 222-240.

MOLSTER, F.J., WATERS, L.B.F.M., TIELENS, A.G.G.M. & BARLOW, M.J. (2002a): Crystalline silicate dust around evolved stars. I. The sample stars. *Astronomy and Astrophysics* **382**, 184-221.

MOLSTER, F.J., WATERS, L.B.F.M., TIELENS, A.G.G.M., KOIKE, C. & CHIHARA, H. (2002c): Crystalline silicate dust around evolved stars. III. A correlations study of the crystalline silicate features. *Astronomy and Astrophysics* **382**, 241-255.

NESTOLA, F., BOFFA BALLARAN, T., LIEBSKE, C., BRUNO, M. & TRIBAUDINO, M. (2006): High-pressure behavior along the jadeite $NaAlSi_2O_6$ – aegirine $NaFeSi_2O_6$ solid solution up to 10 GPa. *Phys. Chem. Minerals* **33**, 417-425.

NESTOLA, F., ROTIROTI, N., BRUNO, M., TRIBAUDINO, M., VAN SMAALEN, S., OHASHI, H. & REDHAMMER, G.J. (2007): Low-temperature behaviour of $NaGaSi_2O_6$. *Am. Mineral.* **92**, 560-569.

OHASHI, H. & SEKITA, M. (1982): Raman spectroscopic study of the Si–O–Si stretching vibration in clinopyroxenes. *J. Japan. Assoc. Mineral., Petrol., Econ. Geol.* **77**, 455-459.

OSTROVSKY, I.A. (1979): The thermodynamics of substances at very high pressures and temperatures and some mineral reactions in the Earth's mantle. *Phys. Chem. Minerals* **5**, 105-118.

PAWLEY, G.S. (1981): Unit cell refinement from powder diffraction scans. *J. Appl. Crystallogr.* **14**, 357-361.

PILATI, T., DEMARTIN, F. & GRAMACCIOLI, C.M. (1996): Lattice-dynamical evaluation of atomic displacement parameters of minerals and its implications: the example of diopside. *Am. Mineral.* **81**, 811-821.

POIRIER, J.-P. (2000): *Introduction to the Physics of the Earth's Interior* (2nd ed.). Cambridge University Press, Cambridge, U.K.

PRENCIPE, M., TRIBAUDINO, M., PAVESE, A., HOSER, A. & REEHUIS, M. (2000): A single-crystal neutron-diffraction investigation of diopside at 10 K. *Can. Mineral.* **38**, 183-189.

PREWITT, C.T. & BURNHAM, C.W. (1966): The crystal structure of jadeite. *Am. Mineral.* **51**, 956- 975.

REDHAMMER, G.J., ROTH, G., PAULUS, W., ANDRÉ, G., LOTTERMOSER, W., AMTHAUER, G., TREUTMANN, W. & KOPPELHUBER-BITSCHNAU, B. (2001): The crystal and magnetic structure of Li-aegirine $LiFe^{3+}Si_2O_6$: a temperature-dependent study. *Phys. Chem. Minerals* **28**, 337-346.

ROBINSON, K., GIBBS, G.V. & RIBBE, P.H. (1971): Quadratic elongation: a quantitative measure of distortion in coordination polyhedra. *Science* **172**, 567-570.

SEARS, V.F. (1992): Neutron scattering lengths and cross sections. *Neutron News* **3**, 26-37.

SHAMIR, N. & SHAKED, H. (1975): The magnetic structure of $CoGeO_3$. *Phys. status solidi (a)* **30**, 315-322.

SHURVELL, H.F., RINTOUL, L. & FREDERICKS, P.M. (2001): Infrared and Raman spectra of jade and jade minerals. *Internet J. Vibrational Spectroscopy* (www.ijvs.com) **5**, 4.

SMITH, D.C. & GENDRON, F. (1997): Archaeometric application of Raman microprobe to the non-destructive identification of two pre-Columbian ceremonial polished "greenstone" axe-heads from Mesoamerica. *J. Raman Spectros.* **28**, 731-738.

SYLVESTER, R.J., KEMPER, F., BARLOW, M.J., DE JONG, T., WATERS, L.B.F.M., TIELENS, A.G.G.M. & OMONT, A. (1999): 2.4–197 μm spectroscopy of OH/IR stars: the IR characteristics of the circumstellar dust in O-rich environments. *Astronomy and Astrophysics* **352**, 587-599.

THOMPSON, J.B. (1970): Geometrical possibilities for amphibole structures: model biopyriboles. *Am. Mineral.* **55**, 292-293.

TOMISAKA, T. & IISHI, K. (1980): Some aspects of the lattice dynamics of diopside. *Mineral. J.* **10**, 84-96.

TRIBAUDINO, M., NESTOLA, F., PRENCIPE, M. & RUNDLOF, H. (2003): A single-crystal neutron-diffraction investigation of spodumene at 54 K. *Can. Mineral.* **41**, 521-527

TUCKER, M.G., DOVE, M.T. & KEEN, D.A. (2000): Direct measurement of the thermal expansion of the Si–O bond by neutron total scattering. *J. Phys.: Condens. Matter* **12**, L425-L430.

VOČADLO, L., BRODHOLT, J., DOBSON, D.B., KNIGHT, K.S., MARSHALL, W.G., PRICE, G.D. & WOOD, I.G. (2002b): The effect of ferromagnetism on the equation of state of Fe_3C studied by first-principles calculations. *Earth Planet. Sci. Lett.* **203**, 567-575.

VOČADLO, L., KNIGHT, K.S., PRICE, G.D. & WOOD, I.G. (2002a): Thermal expansion and crystal structure of FeSi between 4 and 1173 K determined by time-of-flight neutron powder diffraction. *Phys. Chem. Minerals* **29**, 132-139.

WALLACE, D.C. (1972): *Thermodynamics of Crystals*. Wiley, New York, N.Y.

WIEDENMANN, A. & REGNARD, J.-R. (1986): Neutron diffraction study of the magnetic ordering in pyroxenes $Fe_xMg_{1-x}SiO_3$. *Solid State Commun.* **57**, 499-504.

WIEDENMANN, A., REGNARD, J.-R., FILLION, G. & HAFNER, S.S. (1986): Magnetic properties and the magnetic ordering of the orthopyroxenes $Fe_xMg_{1-x}SiO_3$. *J. Phys. C: Solid State Phys.* **19**, 3683-3695.

WILLIS, B.T.M. & PRYOR, A.W. (1975): *Thermal Vibrations in Crystallography*. Cambridge University Press, Cambridge, U.K.

WOOD, I.G., KNIGHT, K.S., PRICE, G.D. & STUART, J.A. (2002): Thermal expansion and atomic displacement parameters of cubic $KMgF_3$ perovskite determined by high-resolution neutron powder diffraction. *J. Appl. Crystallogr.* **35**, 291-295.

WYCKOFF, R.W.G., MERWIN, H.E. & WASHINGTON, H.S. (1925): X-ray diffraction measurements upon the pyroxenes. *Am. J. Sci.* **210**, 383-397.

YANG, HEXIONG & GHOSE, S. (1994): Thermal expansion, Debye temperature and Grüneisen parameter of synthetic $(Fe,Mg)SiO_3$ orthopyroxenes. *Phys. Chem. Minerals* **20**, 575-586.

ZHAO, YUSHENG, VON DREELE, R.B., SHANKLAND, T.J., WEIDNER, D.J., ZHANG, JIANZHONG, WANG, YANBIN & GASPARIK, T. (1997): Thermoelastic equation of state of jadeite $NaAlSi_2O_6$: an energy-dispersive Rietveld refinement study of low symmetry and multiple phases diffraction. *Geophys. Res. Lett.* **24**, 5-8.

Received January 22, 2008, revised manuscript accepted November 3, 2008.